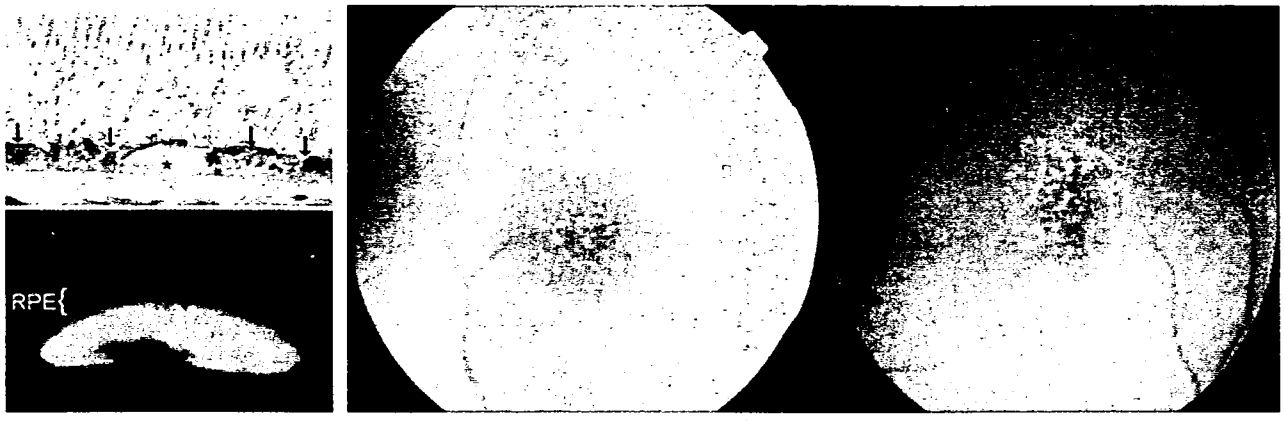

図4　独立行政法人医薬基盤研究所霊長類医科学研究センターで発見された若年性黄斑変性カニクイザルの眼底写真（右）とドルーゼン（左上）およびドルーゼン中の補体活性化（左下）

涙液の網羅的プロテオーム解析，トランスジェニックやノックアウトマウスの眼組織のプロテオーム解析などが行われている。また，最新機器と解析ソフトを利用するとリン酸化，糖，脂質の修飾を受けた蛋白の同定や修飾されたアミノ酸の特定も可能になった。我々は黄斑に特異的な蛋白を探索する過程で，リン酸化蛋白の量的変化を観察している。蛋白修飾の生理的な意味や疾患との関係は今後明らかにされていくと期待される。このような網羅的修飾蛋白の解析はプロテオミクスによって初めて可能になった技術である。

質量分析計にも克服されなければならない弱点が存在する。その一つに質量分析計には定量性が欠けることである。サンプル間に含まれる特定の蛋白について量的変化を高い精度で測定することができない。これまでは電気泳動後のバンドやスポットの濃さとして測定されたり，比較するサンプルを異なる同位体元素でそれぞれラベルして，質量分析計によってラベル化されたペプチドの検出回数として測定されたりする方法が行われてきた。同定した蛋白の定量性について今後の技術開発が望まれている。

おわりに

これまで利用されてきたDNAチップを使った網羅的なトランスクリプトーム解析に加え，これにプロテオーム解析を組み合わせることによって，解析する領域を遺伝子発現から蛋白発現までに広げることが可能になった。DNAチップによって23,000遺伝子の変化を観察し，同時に蛋白の有無を観察することができる。我々も同様な方法によって網膜色素上皮細胞を特異的に増殖させる因子（REF-1/TFPI-2）の作用機序を研究している[10]。この研究では発現量が変化する蛋白間の関係を裏付けるデータとして，遺伝子発現データを利用した。今後はここへ蛋白修飾のデータも加わり，フェノミックスの世界へ一歩近づき，疾患の理解，診断法の開発，さらには治療へと発展するものと期待される。

[文　献]

1) Nakanishi T, et al: Catalogue of soluble proteins in the human vitreous humor: comparison between diabetic retinopathy and macular hole. J Chromatogr B Analyt Technol Biomed Life Sci 776：89-100, 2002.
2) Koyama R, et al: Catalogue of soluble proteins in human vitreous humor by one-dimensional sodium dodecyl sulfate-polyacrylamide gel electrophoresis and electrospray ionization mass spectrometry including seven angiogenesis-regulating factors. J Chromatogr B Analyt Technol Biomed Life Sci 792：5-21, 2003.
3) Yamane K, et al: Proteome analysis of human vitreous proteins. Mol Cell Proteomics 2：1177-1187, 2003.
4) Ouchi M, et al: Proteomic analysis of vitreous from diabetic macular edema. Exp Eye Res 81：176-182, 2005.
5) Hageman GS, et al: Vitronectin is a constituent of ocular drusen and the vitronectin gene is expressed in human retinal pigmented epithelial cells. FASEB J 13：477-484, 1999.

6) Mullins RF, et al: Drusen associated with aging and age-related macular degeneration contain proteins common to extracellular deposits associated with atherosclerosis, elastosis, amyloidosis, and dense deposit disease. FASEB J 14：835-846, 2000.
7) Crabb JW, et al: Drusen proteome analysis: an approach to the etiology of age-related macular degeneration. Proc Natl Acad Sci U S A 99：14682-14687, 2002.
8) Umeda S, et al: Early-onset macular degeneration with drusen in a cynomolgus monkey (Macaca fascicularis) pedigree: exclusion of 13 candidate genes and loci. Invest Ophthalmol Vis Sci 46：683-691, 2005.
9) Umeda S, et al: Molecular composition of drusen and possible involvement of anti-retinal autoimmunity in two different forms of macular degeneration in cynomolgus monkey (Macaca fascicularis). FASEB J 19：1683-1685, 2005.
10) Shibuya M, et al: Proteomic & Transcriptomic Analyses of Retinal Pigment Epithelial Cells Exposed to REF-1/TFPI-2, a Growth Promoting Factor. Invest Ophthal Vis Sci 48：516-521, 2007.

Proteomic and Transcriptomic Analyses of Retinal Pigment Epithelial Cells Exposed to REF-1/TFPI-2

Masahiko Shibuya,[1,2] *Haru Okamoto,*[1] *Takehiro Nozawa,*[3] *Jun Utsumi,*[4] *Venkat N. Reddy,*[5] *Hirotoshi Echizen,*[2] *Yasuhiko Tanaka,*[6] *and Takeshi Iwata*[1]

Purpose. The authors previously reported a growth-promoting factor, REF-1/TFPI-2, that is specific to retinal pigment epithelial (RPE) cells. The purpose of this study was to determine the genes and proteins of human RPE cells that are altered by exposure to TFPI-2.

Methods. Human primary RPE cells were cultured with or without TFPI-2. Cell extracts and isolated RNA were subjected to proteomic and transcriptomic analyses, respectively. Proteins were separated by two-dimensional gel electrophoresis followed by gel staining and ion spray tandem mass spectrometry analyses. Transcriptomic analysis was performed using a DNA microarray to detect 27,868 gene expressions.

Results. Proteomic analysis revealed c-Myc binding proteins and ribosomal proteins L11 preferentially induced by TFPI-2 in human RPE cells. Transcriptomic analysis detected 10,773 of 33,096 probes in the TFPI-2 treated samples, whereas only 2186 probes were detected in the nontreated samples. Among the genes up-regulated by TFPI-2 at the protein level were c-*myc*, Mdm2, transcription factor E2F3, retinoblastoma binding protein, and the *p21* gene, which is associated with the c-*myc* binding protein and ribosomal protein L11.

Conclusions. The mechanisms by which TFPI-2 promotes the proliferation of RPE cells may be associated with augmented c-*myc* synthesis and the activation of E2F in the retinoblastoma protein (Rb)/E2F pathway at the G1 phase of the RPE cells. Activation of ribosomal protein L11 and the Mdm2 complex of the p53 pathway may be counterbalanced by the hyperproliferative conditions. (*Invest Ophthalmol Vis Sci.* 2007;48: 516–521) DOI:10.1167/iovs.06-0434

Retinal pigment epithelial (RPE) cells play important roles in maintaining the homeostasis of the retina. RPE cells, located between the sensory retina and the choroidal blood supply, form a diffusion barrier controlling access to the subretinal space, with the RPE membrane regulating the transport of proteins and controlling the hydration and ionic composition of the subretinal space. The sensitivity and viability of the photoreceptors thus depend on RPE-catalyzed transport activity. Proteins in the RPE cells that function in ionic, sugar, peptide, and water transport have been identified.[1] Damage to RPE cells generally leads to degeneration of the neural retina, as occurs in retinitis pigmentosa and age-related macular degeneration. Transplantation of the healthy retinal pigment cells or embryonic stem cells differentiating into RPE cells would be an ideal therapeutic approach to treat such diseases, and such attempts have been made.[2]

An alternative approach to treat these retinal diseases would be the use of a growth factor that promotes proliferation of the remaining RPE cells in a damaged retina or one that stimulates the regeneration of damaged RPE cells. To find such factor(s), the proteins expressed in human fibroblast cells were fractionated and assayed, leading to the isolation of RPE cell factor-1 (REF-1), which selectively promoted the proliferation of primary human RPE cells.[3]

Subsequently, the cDNA of REF-1 was cloned using information from the N-terminal amino acid sequences, which was identical with the tissue factor pathway inhibitor-2 (TFPI-2).[3] Earlier studies have shown that TFPI-2 is a Kunitz-type serine protease inhibitor[4–6] involved in the regulation of extrinsic blood coagulation[4,7] and in the proliferation, invasion, and metastasis of various types of malignant cells.[4,8–13] Extensive studies on the physiological roles of TEPI-2 have revealed that the ERK/MAPK pathway[13] may be associated with the up-regulation of the *TFPI-2* gene and that DNA methylation[9,10] in certain tumor cell lines may be related to the downregulation of the *TEPI-2* gene. When TFPI-2 is added to the culture medium of vascular smooth muscle cells, it promotes cell proliferation.[14]

Our initial finding that TFPI-2 enhanced RPE proliferation prompted us to question how this was achieved. We applied proteomic and transcriptomic analyses to screen the changes in the expression of the RNAs and proteins in RPE cells and will show that the proliferation promoting activity of TFPI-2 on RPE cells is associated with the regulation of an oncogene product, c-*myc*, and representative cancer repressor proteins retinoblastoma protein (Rb)/E2F and p53.

Materials and Methods

TFPI-2 Treatment of Human RPE Cell Culture

Human primary RPE cells (passage 5) were seeded at a density of 2.5×10^4 cells/0.5 mL per well in 24-well plastic plates (BD Biosciences, Franklin Lakes, NJ) with Dulbecco modified MEM (DMEM; Invitrogen Japan, Tokyo, Japan) containing 15% fetal calf serum (FCS, Invitrogen). TFPI-2 was added to 20 wells with the RPE cells at 10 ng/mL concentrations and was incubated at 37°C for 24 hours for the proteomic samples, and for 6 hours, 12 hours, and 24 hours for the transcriptomic samples. An equal amount of saline was added to 20 wells containing RPE cells for controls. TFPI-2 was donated by Toray Industries, Inc., Tokyo, Japan.

From the [1]Laboratory of Cellular and Molecular Biology, National Institute of Sensory Organs, National Hospital Organization Tokyo Medical Center, Tokyo, Japan; [2]Department of Pharmacotherapy, Meiji Pharmaceutical University, Tokyo, Japan; [3]Analytical Instrument Division, AMR Inc., Tokyo, Japan; [4]R&D Division, Toray Industries, Inc., Tokyo, Japan; [5]Department of Ophthalmology, Kellogg Eye Center, University of Michigan, Ann Arbor, Michigan; and [6]International University of Health and Welfare, Mita Hospital, Tokyo, Japan.

Supported in part by a grant-in-aid from the policy-based Medical Services Foundation.

Submitted for publication April 18, 2006; revised July 17, 2006; accepted December 4, 2006.

Disclosure: **M. Shibuya**, None; **H. Okamoto**, None; **T. Nozawa**, AMR Inc. (F); **J. Utsumi**, Toray Industries, Inc. (F); **V.N. Reddy**, None; **H. Echizen**, None; **Y. Tanaka**, None; **T. Iwata**, None

The publication costs of this article were defrayed in part by page charge payment. This article must therefore be marked "*advertisement*" in accordance with 18 U.S.C. §1734 solely to indicate this fact.

Corresponding author: Takeshi Iwata, Laboratory of Cellular and Molecular Biology, National Institute of Sensory Organs, National Hospital Organization Tokyo Medical Center, 2-5-1 Higashigaoka, Meguro-ku, Tokyo 152-8902, Japan; iwatatakeshi@kankakuki.go.jp.

Investigative Ophthalmology & Visual Science, February 2007, Vol. 48, No. 2

Protein Sample Preparation

To isolate whole cellular protein extracts from cultured RPE cells, the cells were rinsed 3 times with 1× PBS (pH 7.4) and were lysed in a denaturing lysis buffer containing 7 M urea, 2 M thiourea, 4% CHAPS, 40 mM Tris, 0.2% purifier (Bio-Lyte, pH range 3–10; Bio-Rad, Hercules, CA), and 50 mM dithiothreitol (DTT). The collected lysate was then centrifuged at 14,000*g* for 15 minutes at 4°C. Proteins in the supernatant were repeatedly concentrated and precipitated and finally desalinated (Readyprep 2-D Cleanup kit; Bio-Rad). The protein concentration in the RPE samples was determined by a modified Lowry method adapted for use with the lysis buffer.

Two-Dimensional Electrophoresis

Protein samples were separated by a two-dimensional electrophoresis method. A 300-μg protein sample was loaded on immobilized pH gradient (IPG) strips (pH 3–10, 7 cm; pH 4–7, 17 cm; Bio-Rad) by in-gel rehydration at 20°C overnight. For the 7-cm strip, isoelectric focusing (IEF) was used for the first dimension at an initial voltage of 250 V for 15 minutes, increased to 4000 V for 2 hours, and held until 20,000 V/h was reached. For the 17-cm strip, the initial voltage was set at 250 V, as for the 7-cm strip. Then the voltage was increased to 10,000 V for 3 hours and was held until 60,000 V/h was reached. Immediately after IEF, the IPG strips were equilibrated for 20 minutes in buffer containing 6 M urea, 2% SDS, 0.375 M Tris (pH 8.8), and 20% glycerol under a reduced condition with 2% DTT (Bio-Rad), followed by another incubation for 10 minutes in the same buffer under alkylating conditions with 2.5% iodoacetamide (Bio-Rad).[15]

Equilibrated IPG strips were then electophoresed by SDS-PAGE for the second dimension. Images of the chemiluminescent signals were captured and merged with those of protein spots made visible by protein gel stain (Sypro Ruby; Bio-Rad), and the spots corresponding to the immunoreactivity were cut out. To test reproducibility, the experiment was performed twice.

Protein Identification by Mass Spectrometry

Excised gel pieces were rinsed with water and then with acetonitrile and were completely dried for the reduction-alkylation step. They were incubated with 10 mM DTT in 100 mM ammonium bicarbonate for 45 minutes at 56°C, then with 55 mM iodoacetamide in 100 mM ammonium bicarbonate for 30 minutes at room temperature in the dark. The supernatant was removed, and the washing procedure was repeated three times. Finally, the gel pieces were again completely dried before trypsin digestion and were rehydrated in a solution of trypsin (12.5 ng/μL; Promega, Madison, WI) in 50 mM ammonium bicarbonate. The digestion was continued for 16 hours at 37°C, and the extraction step was performed once with 25 mM ammonium bicarbonate, then twice with 5% formic acid, and finally with water. After resuspension in 40 μL solution of aqueous 0.1% trifluoroacetic acid/2% acetonitrile, the samples were analyzed by liquid chromatography coupled to tandem mass spectrometry (LC-MS/MS). For analysis by LC-MS/MS, the tryptic digests were injected by an automatic sampler (HTS-PAL, CTC Analytics, Zwingen, Switzerland) onto a 0.2 × 50-mm capillary reversed-phase column (Magic C18, 3 μm; Michrom BioResources, Inc., Auburn, CA) using an HPLC (Paradigm MS4; Michrom BioResources). Peptides were eluted with a gradient (95% solvent A consisting of 98% H_2O/2% acetonitrile/0.1% formic acid)/5% solvent B (10% H_2O/90% acetonitrile/0.1% formic acid; 0 minute)/35% solvent A/65% solvent B (20 minutes)/5% solvent A/95% solvent B (21 minutes)/5% solvent A/95% solvent B (23 minutes)/95% solvent A/5% solvent B (30 minutes) for 30 minutes at a flow rate of 1.5 μL/min. Peptides were eluted directly into an ion trap mass spectrometer (ESI; Finnigan LTQ; Thermo Electron Corporation, Waltham, MA) capable of data-dependent acquisition. Each full MS scan was followed by an MS/MS scan of the most intense peak in the full MS spectrum with the dynamic exclusion enabled to allow detection of less-abundant peptide ions. Mass spectrometric scan events and HPLC solvent gradients were controlled with the use of a computer program (Paradigm Home; Michrom BioResources).

Total RNA Isolation from RPE Cells

Total RNA was isolated from the cultured RPE cells after 6 hours, 12 hours, and 24 hours with TFPI-2 using a total RNA isolation kit (RNA-Bee-RNA Isolation Reagent; Tel-Test, Friendswood, TX). Total RNA samples were treated with RNase-free DNase (Roche Diagnostics Japan) to minimize genomic DNA contamination.

DNA Microarray Analysis

DNA microarray analysis was performed (AB1700 Chemiluminescent Microarray Analyzer; Applied Biosystems, Foster City, CA). The survey array used (Human Genome Survey Array; Applied Biosystems) contained 33,096 60-mer oligonucleotide probes representing a set of 27,868 individual human genes and more than 1000 control probes. Sequences used for the microarray probe were obtained from curated transcripts (Celera Genomics Human Genome Database), RefSeq transcripts that had been structurally curated from the LocusLink public database, high-quality cDNA sequences from the Mammalian Gene Collection (MGC; http://mgc.nci.nih.gov), and transcripts that were experimentally validated (Applied Biosystems). The 60-mer oligo probes were synthesized using standard phosphoramidite chemistry and solid-phase synthesis and underwent quality control by mass spectrometry. The probes were deposited and covalently bound to a derivatized nylon substrate (2.5 × 3 inches) that was backed by a glass slide by contact spotting with a feature diameter of 180 μm and more than 45 μm between each feature. A 24-mer oligo internal control probe (ICP) was cospotted at every feature with 60-mer gene expression probe on the microarray. Digoxigenin-UTP labeled cRNA was generated and linearly amplified from 1 μg total RNA (Chemiluminescent RT-IVT Labeling Kit, version 2.0; Applied Biosystems) according to the manufacturer's protocol. Array hybridization (two arrays per sample), chemiluminescence detection, image acquisition, and analysis were performed (Chemiluminescence Detection Kit and AB1700 Chemiluminescent Microarray Analyzer; Applied Biosystems) according to the manufacturer's protocol.

Briefly, each microarray was first prehybridized at 55°C for 1 hour in hybridization buffer with blocking reagent. Sixteen micrograms labeled cRNA targets were first fragmented into 100 to 400 bases by incubation with fragmentation buffer at 60°C for 30 minutes, mixed with internal control target (ICT; 24-mer oligo labeled with LIZR fluorescent dye), and hybridized to each prehybrid microarray in 1.5 mL vol at 55°C for 16 hours. After hybridization, the arrays were washed with hybridization wash buffer and chemiluminescence rinse buffer. Enhanced chemiluminescent signals were generated by first incubating the arrays with anti-digoxigenin alkaline phosphatase and enhanced with chemiluminescence enhancing solution and chemiluminescence substrate.

Images were collected from each microarray using the 1700 analyzer equipped with a high-resolution, large-format CCD camera, including 2 "short" chemiluminescent images (5-second exposure length each) and 2 "long" chemiluminescent images (25-second exposure length each) for gene expression analysis, two fluorescent images for feature finding and spot normalization, and two quality control images for spectrum cross-talk correction. Images were quantified, corrected for background and spot, and spatially normalized.

Data Analysis

MS data were identified with the use of a protein search program (BioWorks 3.2; Thermo Electron Corporation, Waltham, MA). For protein database searches, the same program was used to create centroid peak lists from the raw spectra. These peak lists were then submitted for database searching (BioWorks). The identity of the samples was searched from databases (nrNCBI [www.ncbi.nlm.nih.gov]) that extracted proteins and were restructured; search terms included human and *Homo sapiens*. Differentially expressed proteins were further analyzed for related genes and proteins using natural language processing software (Pubgene database; PubGene Inc., Boston, MA) and data mining software of gene expression (OmniViz; OmniViz, Inc., Maynard, MA).

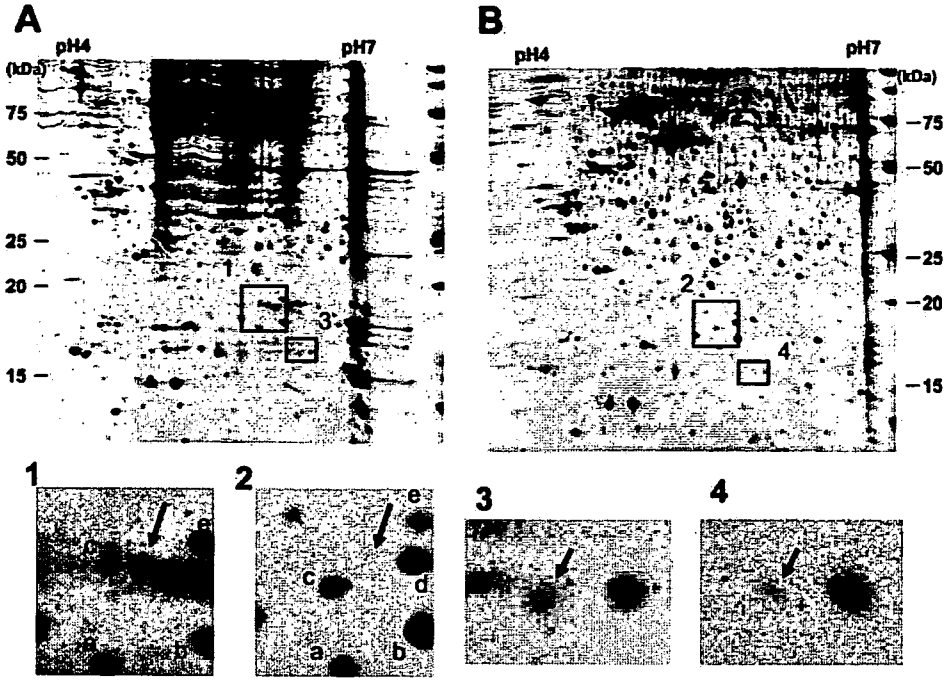

FIGURE 1. Two-dimensional gel electrophoresis of human RPE cells culture with (A) and without (B) TFPI-2. Spots corresponding to proteins whose expression is dependent on the presence of TFPI-2 in the culture medium are indicated by the *arrows* (*insets*). Proteins were detected by SYPRO Ruby staining. Spots corresponding to the differentially expressed proteins indicated by *arrows* (1 vs. 2 and 3 vs. 4) were subsequently subject to the LC-MS/MS analysis so that proteins could be identified.

RESULTS

Proteome Analysis of RPE Cells Treated with TFPI-2

To determine the mechanisms responsible for the proliferation-promoting activity of TFPI-2 on RPE cells, protein synthesis and RNA expression were determined before and after TFPI-2 exposure. Differentially expressed proteins in the primary human RPE cells in response to TFPI-2 were identified by two-dimensional electrophoresis (Fig. 1). Samples were initially separated using IPG at a pH range of 3 to 10 to observe the full distribution of protein spots. The pH range was then narrowed to 4 to 7 to obtain higher resolution for spot picking. Consequently, approximately 480 spots were identified in the whole gel. We then focused on molecular weight less than 25 kDa, which is easy to check for changes. Ten spots considered differentially expressed in the two-dimensional gel were collected and subjected to LC-MS/MS analysis. Among the identified proteins, ribosomal protein L11 (RPL11; Fig. 1-1) and c-Myc binding protein (MYCBP; Fig. 1-3), known for regulating cell proliferation, were identified.[16] These two proteins, identified by LC-MS/MS analysis and data analysis software (Bioworks 3.2), were consistent with those estimated from the results of two-dimensional electrophoresis (Table 1).

Transcriptomic Analysis of RPE Cells Treated with TFPI-2

The expression of 8134 genes in RPE cells was analyzed using DNA microarray with and without TFPI-2 exposure for 6 hours, 12 hours, and 24 hours. Signal normalization was performed for six independent DNA microarray chips according to the manufacturer's protocol. Genes differentially expressed by more than threefold were considered significant and were selected for further analysis. Among the 33,096 possible probes, 10,773 probes were detected in the RPE cells incubated with TFPI-2, whereas only 2186 probes were detected without TFPI-2. Based on expression levels at the three time points (6 hours, 12 hours, and 24 hours), the time-dependent expression pattern of each gene was calculated and clustered with other genes with similar expression patterns using data mining software (OmniViz). Data analysis resulted in 38 clusters of genes that either increased or decreased their expression levels by more than twofold after TFPI-2 (Fig. 2). Nineteen genes were upregulated in 5 clusters, 108 genes in 16 clusters, and 717 genes in 22 clusters at 6 hours, 12 hours, and 24 hours, respectively. For downregulated genes, 30 genes in 16 clusters, 119 genes in 19 clusters, and 3 genes in 19 clusters were observed after 6 hours, 12 hours, and 24 hours, respectively. Transcriptomic analysis revealed significantly more genes differentially expressed at the transcriptional level than at the proteome level.

DISCUSSION

Proteins and genes whose expression was upregulated or downregulated after exposure to TFPI-2 were analyzed in human RPE cells to study the proteomic and transcriptomic changes. Protein and gene expression profiles for human RPE cells have been reported by West et al.,[17] who identified 278 proteins, and Cai et al.,[18] who reported 5580 ± 84 genes expressed in adult human RPE and ARPE19 cell lines using a DNA chip with 12,600 probes (Human U95Av2; Affymetrix, Santa Clara, CA). Our study showed changes in the expression of 8134 of 27,868 genes. DNA microarray analyses were simul-

TABLE 1. Two-Dimensional Gel Spots Identified by Mass Spectrometry

Protein	Number of AA	Peptide Residues	Identified Peptide from Database	MW	Score	Accession Number
c-Myc binding protein	167	108–117	TAEDAKDFFK	18642.6	10.13	1731809
Ribosomal protein L11	177	88–94	VREYELR	20125.1	20.21	14719845

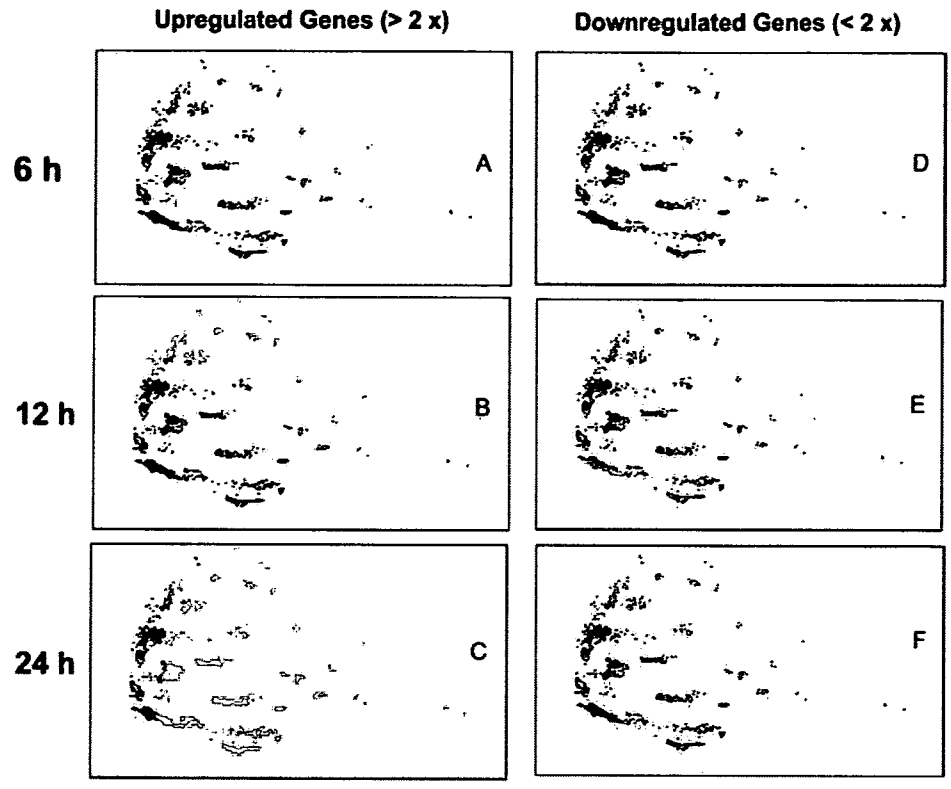

FIGURE 2. Differentially expressed genes detected by DNA array are plotted as clusters. Differentially expressed genes whose expression level was increased by more than twofold (A–C) or was reduced by more than 0.5-fold (D–F) in RPE cells treated with TFPI-2 at incubation times of 6 hours, 12 hours, and 24 hours compared with the control cells are shown. Expression profile analysis revealed different gene expression patterns at each incubation time.

taneously performed at three time points (6 hours, 12 hours, and 24 hours) to monitor the course of expression of the possible 27,868 genes in human RPE cells exposed and not exposed to TFPI-2. This study was conducted at the translational and the transcriptional levels to complement the disadvantages of each method.

Raw gene expression data were further analyzed with data mining software (OmniViz) to obtain an overall picture of the transcriptional changes induced by TFPI-2 in human primary RPE cells. Genes whose expressions were changed by more than twofold were clustered into 38 groups showing a change of expression at each time point (Fig. 2). The number of genes upregulated at each time point was considerably higher than the number that was downregulated. A small number of genes was triggered by TFPI-2 treatment at 6 hours, before the major changes occurred at 24 hours. Among the initially upregulated genes were reticulon 4 interacting protein 1, phospholipase C, delta 1, granzyme M (lymphocyte met-ase 1; *GZMM*), and mitochondrial ribosomal protein L41 (*MRPL41*).

Proteomics analysis simultaneously performed at 24 hours identified two differentially expressed proteins, the c-*myc* binding protein (MYCBP) and the ribosomal protein L11 (RPL11). MYCBP and RPL11 (Fig. 3) are well known to regulate cell cycling through the Rb/E2F pathway and the p53 pathway, respectively. MYCBP stimulates c-*myc* transcription through the retinoblastoma protein (Rb)/E2F pathway (see Fig. 5). Sears et al.[19] reported that activation of Myc increased the signal transduction of the cyclin D/cdk4 and cyclin E/cdk2 pathways. Activation of these pathways inactivates Rb after phosphorylation and E2F dissociation, which then promotes RPE cells to go into the S-phase of the cell cycle. The twofold transcriptional increase of *Rb* and *E2F3* in TFPI-2 exposed cells compared with control at 24 hours supports this hypothesis (Figs. 4C, 4F).

Concomitantly, the expressions of Rb and Mdm2 were upregulated twofold in growth-stimulated cells compared with control cells. Because Rb is associated with the negative regulation of the G_1-phase of the cell cycle, the enhanced expres-

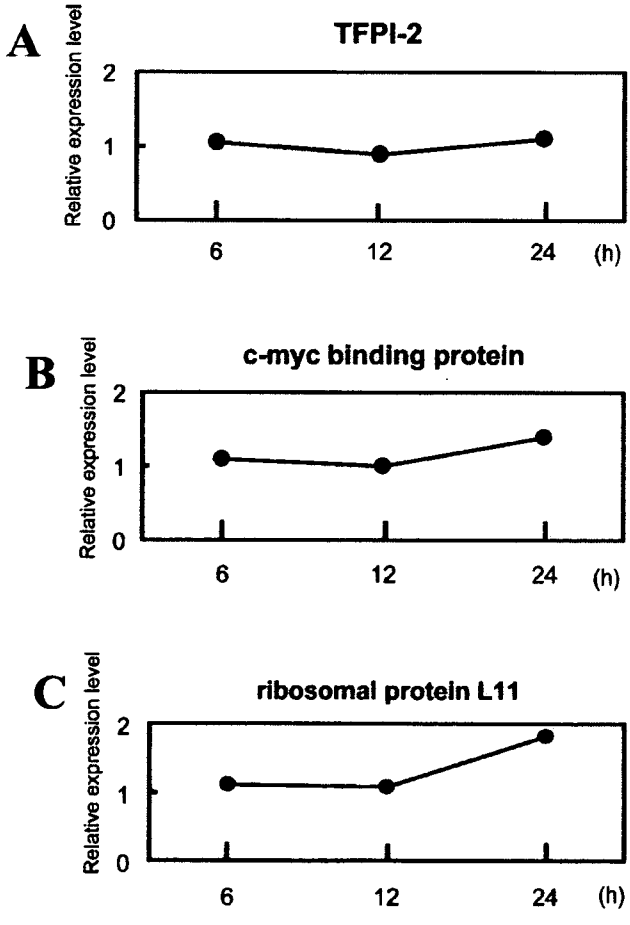

FIGURE 3. Time course of gene expression for TFPI-2 (A), c-*myc* binding protein (B), and ribosomal protein L11 (C) in the cultured human RPE cells after exposure to TFPI-2.

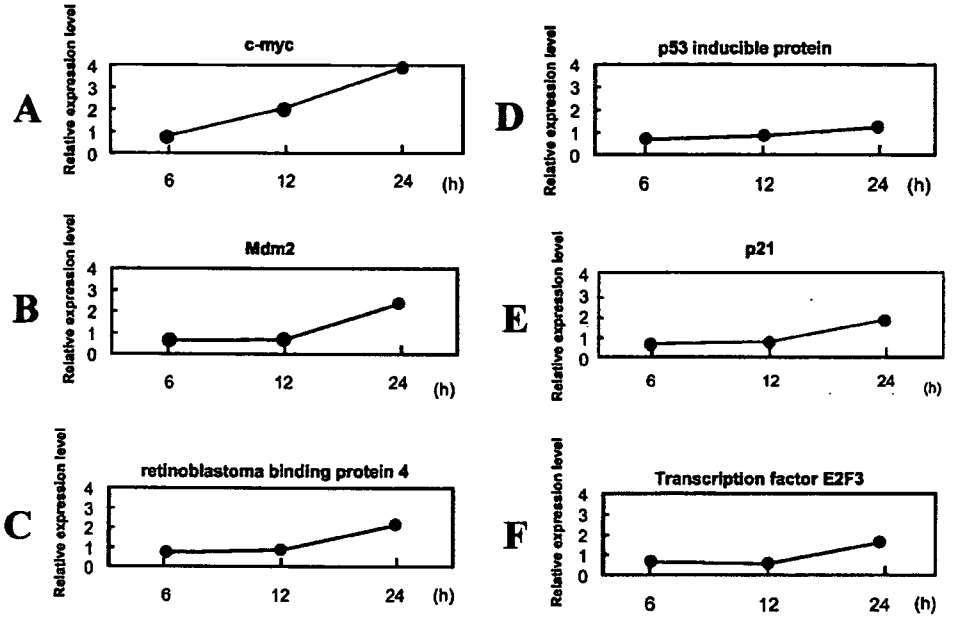

FIGURE 4. Time courses of protein expression patterns for c-*myc* (A), Mdm2 (B), retinoblastoma binding protein 4 (C), p-53 inducible protein (D), p21 (E), and transcription factor E2F3 in the cultured human RPE cells after exposure to TFPI-2.

sion of *Mdm2* might have been involved in the augmented degradation of Rb through the ubiquitin/proteasome-dependent pathway. Recently, Uchida et al.[20] suggested that Mdm2 regulates the function of RB through the ubiquitin-dependent degradation of RB.

The *Rb* gene was the first identified tumor-suppressor gene,[21] and it was recognized as a central component of a signaling pathway that controlled cell proliferation. Specifically, the D-type G_1 cyclins, together with their associated cyclin-dependent kinases (CKDs) Cdk4 and Cdk6, initiated the phosphorylation of Rb and Rb family members, inactivating their capacity to interact with the E2F transcription factors (Fig. 5).[19] This phosphorylation leads to an accumulation of E2F1, E2F2, and E2F3a, which activate the transcription of a large number of genes essential for DNA replication and further cell cycle progression.[22–26] Among the E2F targets are genes encoding a second class of G_1 cyclins, cyclin E, and the associated kinase Cdk2 (Fig. 5).[19] The activation of cyclin E/Cdk2 kinase activity by E2F leads to further phosphorylation and inactivation of Rb, further enhancing E2F activity and increasing the accumulation of cyclin E/Cdk2 (Fig. 5).[19] This feedback loop, which leads to a continual inactivation of *Rb* independent of the action of cyclin D/Cdk4—defined as a junction in cell proliferation response when passaged through the cell cycle—becomes growth factor independent.[25,26] The activity of the G_1 Cdks is negatively regulated by a family of cyclin-dependent kinase inhibitors (CKIs), including $p21^{WAF1}$, $p27^{Kip1}$, and the $p16^{INK4a}$ family.[27] The three upregulated E2Fs associate exclusively with Rb and appear to play a positive role in cell cycle progression.[19]

RPL11 binds the mouse double-minute 2 (Mdm2 is the mouse homologue of Hdm2 in humans) protein with other ribosomal proteins (L23 and L5) to form a complex to inhibit ubiquitin-dependent degradation of p53.[28–30] The RPL11 protein is expressed in ARPE-19 cells.[31] Inhibition of p53 degradation leads to p21 signaling, which participates in the G_1

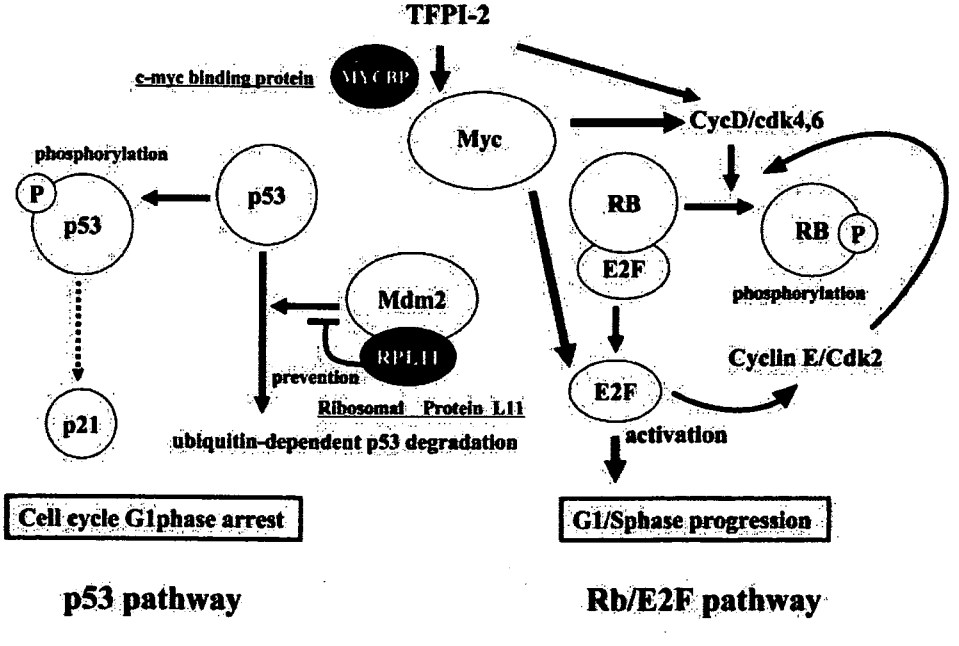

FIGURE 5. Hypothetical network of various genes and proteins associated with the growth-promoting effect of TFPI-2 on the human RPE cells. *Arrows*: stimulatory signals. *Straight* and *dotted lines*: inhibitory effects.

arrest of the cell cycle but also negatively regulates cell proliferation (Fig. 5).[30,32-34] In support of this hypothesis, *p21* transcription was increased by twofold after 24 hours by TFPI-2.

The *p53* gene mediates a major tumor-suppression pathway in mammalian cells and is frequently altered in human tumors.[30] Its function is kept at a low level during normal cell growth and is activated in response to various cellular stresses by acting as a sequence-specific transcription factor.[30] The p53 protein induces cell cycle arrest or apoptosis.[30]

Shinoda et al.[14] reported cell growth proliferation of vascular smooth muscle endothelial cells by a purified mitogenic substance from human umbilical vein endothelial cells, later identified as TFPI-2. These authors showed the rapid activation of mitogen-activated protein kinase (MAPK) by TFPI-2 and the induced activation of proto-oncogene *c-fos* mRNA in smooth muscle cells.[14] They concluded that *c-fos* activation was initiated by MAPK based on MAPK inhibitor PD098059 suppression.

In conclusion, the results of proteomic and transcriptomic analyses suggest that the proliferation of RPE cells induced by TFPI-2 is regulated through the Rb/E2F, p53, and Ras/Raf/MAPK pathways. We and others[3,35] have reported a transcript of TFPI-2 in the mRNA of RPE cells. It is now reasonable to expect that RPE cells are able to self-proliferate by generating TFPI-2. Additional studies are needed to determine whether TFPI-2 can act as such an autocrine factor and can be modified for future treatment of the dry-type age-related macular degeneration and of retinitis pigmentosa.

References

1. Hughes BA, Gallemore RP, Miller SS. Transport mechanisms in the retinal pigment epithelium. In: Marmor MF, Wolfensberger TJ, eds. *The Retinal Pigment Epithelium: Function and Disease*. New York: Oxford University Press; 1998:103-134.
2. Haruta M. Embryonic stem cells: potential source for ocular repair. *Semin Ophthalmol*. 2005;20:17-23.
3. Tanaka Y, Utsumi J, Matsui M, et al. Purification, molecular cloning, and expression of a novel growth-promoting factor for retinal pigment epithelial cells, REF-1/TFPI-2. *Invest Ophthalmol Vis Sci*. 2004;45:245-252.
4. Chand HS, Foster DC, Kisiel W. Structure, function and biology of tissue factor pathway inhibitor-2. *Thromb Haemost*. 2005;94: 1122-1130.
5. Schmidt AE, Chand HS, Cascio D, et al. Crystal structure of Kunitz domain 1 (KD1) of tissue factor pathway inhibitor-2 in complex with trypsin: implications for KD1 specificity of inhibition. *J Biol Chem*. 2005;280:27832-27838.
6. Chand HS, Schmidt AE, Bajaj SP, et al. Structure-function analysis of the reactive site in the first Kunitz-type domain of human tissue factor pathway inhibitor-2. *J Biol Chem*. 2004;279:17500-17507.
7. Sprecher CA, Kisiel W, Mathewes S, et al. Molecular cloning, expression, and partial characterization of a second human tissue-factor-pathway inhibitor. *Proc Natl Acad Sci USA*. 1994;91:3353-3357.
8. Yanamandra N, Kondraganti S, Gondi CS, et al. Recombinant adeno-associated virus (rAAV) expressing TFPI-2 inhibits invasion, angiogenesis and tumor growth in a human glioblastoma cell line. *Int J Cancer*. 2005;115:998-1005.
9. Rollin J, Iochmann S, Blechet C, et al. Expression and methylation status of tissue factor pathway inhibitor-2 gene in non-small-cell lung cancer. *Br J Cancer*. 2005;92:775-783.
10. Konduri SD, Srivenugopal KS, Yanamandra N. Promoter methylation and silencing of the tissue factor pathway inhibitor-2 (TFPI-2), a gene encoding an inhibitor of matrix metalloproteinases in human glioma cells. *Oncogene*. 2003;22:4509-4516.
11. Santin AD, Zhan F, Bignotti E, et al. Gene expression profiles of primary HPV16- and HPV18-infected early stage cervical cancers and normal cervical epithelium: identification of novel candidate molecular markers for cervical cancer diagnosis and therapy. *Virology*. 2005;331:269-291.
12. Sato N, Parker AR, Fukushima N, et al. Epigenetic inactivation of TFPI-2 as a common mechanism associated with growth and invasion of pancreatic ductal adenocarcinoma. *Oncogene*. 2005;24: 850-858.
13. Kast C, Wang M, Whiteway M. The ERK/MAPK pathway regulates the activity of the human tissue factor pathway inhibitor-2 promoter. *J Biol Chem*. 2003;278:6787-6794.
14. Shinoda E, Yui Y, Hattori R, et al. Tissue factor pathway inhibitor-2 is a novel mitogen for vascular smooth muscle cells. *J Biol Chem*. 1999;274:5379-5384.
15. Bahk SC, Lee SH, Jang JU, et al. Identification of crystallin family proteins in vitreous body in rat endotoxin-induced uveitis: involvement of crystallin truncation in uveitis pathogenesis. *Proteomics*. 2006;6:3436-3444.
16. Taira T, Maëda J, Onishi T, et al. AMY-1, a novel C-MYC binding protein that stimulates transcription activity of C-MYC. *Genes Cells*. 1998;3:549-565.
17. West KA, Yan L, Shadrach K, et al. Protein database, human retinal pigment epithelium. *Mol Cell Proteomics*. 2003;2:37-49.
18. Cai H, Del Priore LV. Gene expression profile of cultured adult compared to immortalized human RPE. *Mol Vis*. 2006;12:1-14.
19. Sears RC, Nevins JR. Signaling networks that link cell proliferation and cell fate. *J Biol Chem*. 2002;277:11617-11620.
20. Uchida C, Miwa S, Kitagawa K, et al. Enhanced Mdm2 activity inhibits pRB function via ubiquitin-dependent degradation. *EMBO J*. 2005;24:160-169.
21. Hanahan D, Weinberg RA. The hallmarks of cancer. *Cell*. 2000; 100:57-70.
22. Dyson N. The regulation of E2F by pRB-family proteins. *Genes Dev*. 1998;12:2245-2262.
23. Nevins JR. Toward an understanding of the functional complexity of the E2F and retinoblastoma families. *Cell Growth Differ*. 1998; 9:585-593.
24. Harbour JW, Dean DC. Rb function in cell-cycle regulation and apoptosis. *Nat Cell Biol*. 2000;2:E65-E67.
25. Dou QP, Levin AH, Zhao S, Pardee AB. Cyclin E and cyclin A as candidates for the restriction point protein. *Cancer Res*. 1993;53: 1493-1497.
26. Pardee AB. A restriction point for control of normal animal cell proliferation. *Proc Natl Acad Sci USA*. 1974;71:1286-1290.
27. Sherr CJ, Roberts JM. CDK inhibitors: positive and negative regulators of G1-phase progression. *Genes Dev*. 1999;13:1501-1512.
28. Krystof V, McNae IW, Walkinshaw MD. Antiproliferative activity of olomoucine II, a novel 2,6,9-trisubstituted purine cyclin-dependent kinase inhibitor. *Cell Mol Life Sci*. 2005;62:1763-1771.
29. Dai MS, Lu H. Inhibition of MDM2-mediated p53 ubiquitination and degradation by ribosomal protein L5. *J Biol Chem*. 2004;279: 44475-44482.
30. Zhang Y, Wolf GW, Bhat K, et al. Ribosomal protein L11 negatively regulates oncoprotein MDM2 and mediates a p53-dependent ribosomal-stress checkpoint pathway. *Mol Cell Biol*. 2003;23:8902-8912.
31. Rao KC, Palamalai V, Dunlevy JR, et al. Peptidyl-Lys metalloendopeptidase-catalyzed ^{18}O labeling for comparative proteomics: application to cytokine/lipolysaccharide-treated human retinal pigment epithelium cell line. *Mol Cell Proteomics*. 2005;4:1550-1557.
32. Chao C, Saito S, Kang J. p53 transcriptional activity is essential for p53-dependent apoptosis following DNA damage. *EMBO J*. 2000; 19:4967-4975.
33. Bai F, Matsui T, Ohtani-Fujita N, et al. Promoter activation and following induction of the p21/WAF1 gene by flavone is involved in G1 phase arrest in A549 lung adenocarcinoma cells. *FEBS Lett*. 1998;437:61-64.
34. Nyunoya T, Powers LS, Yarovinsky TO. Hyperoxia induces macrophage cell cycle arrest by adhesion-dependent induction of p21Cip1 and activation of the retinoblastoma protein. *J Biol Chem*. 2003;278:36099-360106.
35. Ortego J, Escribano J, Coca-Prados M. Gene expression of protease and protease inhibitors in the human ciliary epithelium and ODM-2 cells. *Exp Eye Res*. 1997;65:289-299.

Molecular Vision 2007; 13:545-48 <http://www.molvis.org/molvis/v13/a58/>
Received 9 November 2006 | Accepted 23 March 2007 | Published 4 April 2007

HTRA1 promoter polymorphism predisposes Japanese to age-related macular degeneration

Tsunehiko Yoshida,[1] Andrew DeWan,[2] Hong Zhang,[2] Ryosuke Sakamoto,[1] Haru Okamoto,[1] Masayoshi Minami,[1] Minoru Obazawa,[1] Atsushi Mizota,[3] Minoru Tanaka,[3] Yoshihiro Saito,[4] Ikue Takagi,[5] Josephine Hoh,[2] Takeshi Iwata[1]

(The first four authors contributed equally to this publication)

[1]National Institute of Sensory Organs, National Hospital Organization Tokyo Medical Center, Tokyo, Japan; [2]Department of Epidemiology and Public Health, Yale University School of Medicine, 60 College Street, New Haven CT 06520, [3]Department of Ophthalmology, Juntendo University Urayasu Hospital, Chiba, [4]Division of Ophthalmology, National Hospital Organization Osaka Medical Center, Osaka, [5]Division of Ophthalmology, National Hospital Organization Kyushu Medical Center, Fukuoka, Japan

Purpose: To study the effect of candidate single nucleotide polymorphisms (SNPs) on chromosome 10q26, recently shown to be associated with wet age-related macular degeneration (AMD) in Chinese and Caucasian cohorts, in a Japanese cohort.

Methods: Using genomic DNA isolated from peripheral blood of wet AMD cases and age-matched controls, we genotyped two SNPs, rs10490924, and rs11200638, on chromosome 10q26, 6.6 kb and 512 bp upstream of the *HTRA1* gene, respectively, using temperature gradient capillary electrophoresis (TGCE) and direct sequencing. Association tests were performed for individual SNPs and jointly with SNP complement factor H (CFH) Y402H.

Results: The two SNPs, rs10490924 and rs11200638, are in complete linkage disequilibrium (D'=1). Previous sequence comparisons among seventeen species revealed that the genomic region containing rs11200638 was highly conserved while the region surrounding rs10490924 was not. The allelic association test for rs11200638 yielded a p-value $<10^{-11}$. SNP rs11200638 conferred disease risk in an autosomal recessive fashion: Odds ratio was 10.1 (95% CI 4.36, 23.06), adjusted for SNP CFH 402, for those carrying two copies of the risk allele, whereas indistinguishable from unity if carrying only one risk allele.

Conclusions: The *HTRA1* promoter polymorphism, rs11200638, is a strong candidate with a functional consequence that predisposes Japanese to develop neovascular AMD.

Japanese patients are predominantly affected with vascular or "wet" AMD with little or no drusen deposition, in contrast to the Caucasian population which has a higher prevalence of drusen formation and the dry form of the disease. Association between the complement factor H (CFH) Y402H polymorphism (CFH 402) and age-related macular degeneration (AMD) has been shown in twelve or so different Caucasian populations [1,2]. However, that association failed to be replicated in Japanese populations, in which no control individual was found to be homozygous for the risk allele [3,4].

HTRA1 is a member of the heat shock serine proteases and is up-regulated by cellular stress. *HTRA1* is expressed in both the human and mouse retina [5,6]. Recently a promoter single nucleotide polymorphism (SNP) rs11200638 in *HTRA1* was shown to be highly associated with wet AMD [6,7]. Furthermore, *HTRA1* resides in a region of chromosome 10q26 that has been implicated as the "top" candidate region for AMD. Here we test two SNPs, rs10490924 (6.6 kb upstream of *HTRA1*), and rs11200638, for their association to wet AMD in a Japanese population.

Correspondence to: Josephine Hoh, Department of Epidemiology and Public Health, Yale University, 60 College Street, Room 416, New Haven CT 06520, Phone: (203) 785-6831; FAX: (203) 785-6279; email: josephine.hoh@yale.edu

METHODS

We genotyped 88 neovascular AMD cases and 97 AMD-free age-matched controls for SNPs rs10490924 and rs11200638. Case and control individuals were the same as our previous CFH association study [3] with all cases being characterized as AMD grade 5B [1]. Among cases the mean age was 74.8 years (standard deviation: s.d. 8.8 years) and 70.5% male; among controls the mean age was 71.1 years (s.d. 9.1 years), and 38.1% male. Informed consent was obtained from all participants, and the procedures used conformed to the tenets of the Declaration of Helsinki. Genotyping was performed as described previously [3]. Briefly, PCR was performed using primers designed to amplify the genomic region containing each SNP (rs10490924 forward: 5'-GGT GGT TCC TGT GTC CTT CA-3', reverse: 5'-GGG GTA AGG CCT GAT CAT CT-3'; rs11200638 forward: 5'-CGG ATG CAC CAA AGA TTC TCC-3', reverse: 5'-TTC GCG TCC TTC AAA CTA ATG G-3'). Following amplification, genotype determination was performed on the PCR products using either temperature gradient capillary electrophoresis (TGCE; Reveal SpectruMedix,

State College, PA) or through direct sequencing using CEQ2000XL DNA analysis system (Beckman Coulter, Fullerton, CA).

Hardy Weinberg equilibrium (HWE) χ^2 values in the entire sample and controls only were calculated to identify possible genotyping errors. No extreme deviations (χ^2>50) were observed (Table 1). Linkage disequilibrium (LD) was measured by the D' value. For each SNP, Pearson's χ^2 tests with one degree of freedom for association were performed. Odds ratios (OR), population attributable risks (PAR), and their respective confidence intervals were calculated, formula in [8].

Previous functional data lead us to focus further analyses on rs11200638 [6,7]. Joint ORs for two SNPs (rs11200638 and CFH 402, previously genotyped) were calculated using standard methods [9]. Marginal ORs and their confidence intervals for the two SNP were calculated using logistic regression with SNP CFH 402 and rs11200638 as independent variables [9]. PARs were calculated using standard methods [9]. Confidence intervals around the PARs were constructed using 999 bootstrap replicates. To control for confounding, the Mantel-Hanzel test for association with two variables was used [9]. Four genotypic models were considered (Full, Recessive, Multiplicative, and Dominant) and the Aikake information criterion (AIC) was utilized to assess the fit of each model. All R scripts used in the analysis are available upon request.

RESULTS

SNP rs11200638, approximately 6.1 kb downstream of the surrogate SNP rs10490924, resides in the promoter of the *HTRA1* serine protease gene (512 base pairs upstream of transcriptional start site). These two SNPs were in almost complete linkage disequilibrium (LD) and showed strong association with AMD in the Hong Kong study [6] and in a Caucasian population from Utah [7].

In our cohort, the two SNPs were also in complete LD, from which only two major (frequency >5%) haplotypes, one predominant in cases and one in controls, were observed. Disease association tests yielded p-values of 4.74×10^{-11} and 1.79×10^{-12} for rs10490924 and rs11200638, respectively (Table 1). Given the previous evidence of higher conservation across species [6] and the functional consequence of rs11200638 on *HTRA1* expression [6,7], additional analyses focused on this SNP.

Reanalyzing the original CFH genotype data, we found the OR covered unity (Table 2) and all interval estimates of PAR for CFH 402 variants under the four genotypic models included zero (Table 3). Of the four models, the best fit to the *HTRA1* SNP genotypic effects, as assessed by Akaike's information criterion, was the recessive model, from which the risk genotype was AA and non-risk was GG and GA (Table 3). Under the framework of recessive rs11200638 and the two observed genotypes for CFH 402, no interaction was detected between the two SNPs based on the likelihood ratio test (Table 3). Odds ratios for different genotypes of rs11200638 do not vary a great deal depending on the CFH 402 genotypes, and vice versa (Table 2). In fact, the OR curves shown in Figure 1 indicate a "removable" interaction between the two SNPs, in which the original two OR curves become parallel (i.e. no

Table 1. Association of chromosome 10q26 single nucleotide polymorphisms with age-related macular degeneration

Attribute	rs10490924 (G/T)	rs11200638 (G/A)
HWE χ^2-combined	5.4	7.6
-controls only	0.98	0.88
Risk allele	T	A
Frequency in case	0.68	0.69
Frequency in control	0.33	0.32
Allelic association χ^2 nominal p-value	4.74E-11	1.79E-12

To examine genotyping errors, Hardy Weinberg Equilibrium (HWE) χ^2 values are computed with cases and controls combined and controls alone. The age range is 51 to 90 years old with mean 74.8 and standard deviation (s.d.) 8.81 in cases, and 50 to 88 years old with mean 71.1 and s.d. 9.08 in controls.

Table 2. Odds ratios for the joint and marginal effects of single nucleotide polymorphisms complement factor H 402 and rs11200638 on age-related macular degeneration

	rs11200638		
CFH 402	GG/GA	AA	CFH 402 risk (adjusted for rs11200638)
TT	1	7.92	1
CT	1.11	30.52	1.41 (95% CI: 0.54,3.74)
rs11200638 risk adjusted for CFH	1	10.02; 95% CI: 4.36,23.06	

CFH indicates complement factor H. Joint odds ratios were calculated from standard formulae. Marginal odds ratios and 95% confidence intervals were calculated using logistic regression (see Methods) with each SNP was adjusted for the other.

interaction after transformation with a logarithmic function). Overall, after adjusting for the CFH 402 SNP, individuals carrying the risk homozygote AA of rs11200638 are greater than 10 times more likely to have AMD than those with the other genotypes (Table 2).

DISCUSSION

These data reconfirm the association of the *HTRA1* promoter SNP rs11200638, independent of the CFH 402 polymorphism, with wet AMD. The present study genotyped two previously identified disease associated SNPs in the chromosome 10q26 region. Both SNPs showed similar significance levels. The first SNP, rs10490924, resides in the hypothetical locus, LOC387715. Several studies have found significant association between AMD and this SNP [10-12]. So far only one transcript from this hypothetical locus has been identified in one experiment. No study has identified the transcript or protein in the retina, much less identified a change in the protein as a result of the SNP. Additionally, sequence comparisons of seventeen species presented in DeWan et al. show higher sequence

Table 3. Two-way analyses of complement factor H 402 and rs11200638

Model for rs11200638	PAR%		(95% CI)		M-H test: p-value LRT p-value	AIC value
	CFH 402	rs11200638	CFH 402	rs11200638		
Full	3.4 (0, 9.7)	58.3 (50.5, 64.1)	0.07	8.30E-08	0.03	221.8
Recessive	4.6 (0, 10.7)	44 (40.5, 54.0)	0.23	6.20E-09	0.12	221.5
Multiplicative	1.7 (0, 7.8)	79.8 (73.0, 88.1)	*	*	0.02	225.7
Dominant	2.2 (0, 13.7)	58.6 (43.9, 78.9)	0.91	5.80E-04	0.1	246.9

Four genotypic models for rs11200638 are considered: Let r0, r1, and r2 be the marginal relative risks for genotypes GG, GA, and AA. Then, recessive model implies r0=r1; multiplicative model implies r1=r0r2; dominant model implies r2=r1; full model does not have any restriction on relative risks except that r0, r1, r2>0. The 95% confidence intervals (CI) of population attributable risk (PAR) were obtained via a bootstrap re-sampling method with 999 replicates. Mantel-Hanzel (M-H) tests are conducted for one SNP association adjusted for the other SNP; likelihood ratio tests (LRT) for joint single nucleotide polymorphism (SNP) association under a two-way multiplicative model: the relative risk (or OR) for any genotype pair (A, B) relative to the baseline pair (A0, B0) is the product of relative risk (or OR) of A relative to A0 and that of B relative to B0. AIC denotes the Akaike's information criterion to access goodness-of-fit for the rs11200638 model.

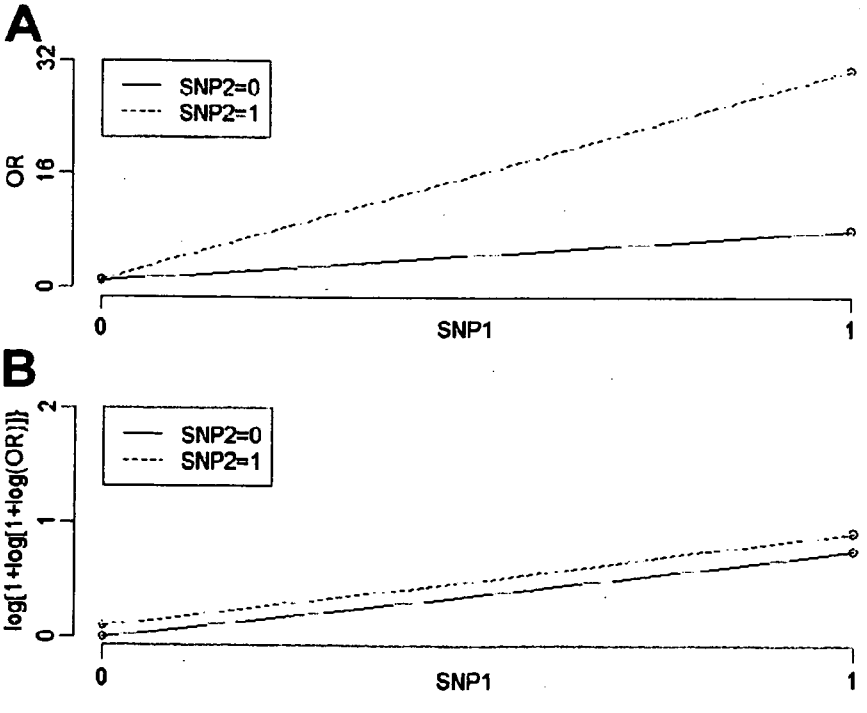

Figure 1. Odds ratio plots for two single nucleotide polymorphisms. Joint odds ratio plots for the single nucleotide polymorphisms (SNPs), complement factor H (CFH) 402, and rs11200638 before and after log transformation showing that the apparent interaction is a "removable" effect. SNP1=CFH 402: 0 is for TT and 1 is for CT; SNP2=rs11200638: 0 is for GG/GA and 1 is for AA. **A**: Original odds ratio (OR) curves: Height difference on the left is 1.11-1=0.11; height difference on the right is 30.52-7.92=22.60; slope for SNP2=0 is 7.92-1=6.92; slope for SNP2=1 is 30.52-1.11=29.41. **B**: Log(1+log(1+log)) transformation of the original OR.

conservation surrounding rs11200638 compared to that around rs10490924 [6]. *HTRA1* is expressed in the retina in humans [5] and mouse [6]. Computational analysis of the *HTRA1* promoter indicate that this SNP resides in a CpG island and may result in a change in the binding site for transcription factors AP2 and SRF [6]. Preliminary functional data suggest that individuals homozygous for the risk-allele at rs11200638 exhibit increased expression of *HTRA1* [6,7]. Therefore, given the existing functional data, it appears as if the *HTRA1* promoter polymorphism, rs11200638, is likely the underlying functional polymorphism in the 10q26 region. However, the mechanism to neovascularization is yet to be understood and will require intense investigation to uncover its link to the wet form of AMD.

ACKNOWLEDGEMENTS

This work was supported in part by grants from the National Institutes of Health and by awards from the Macular Vision Research Foundation and the Ellison Medical Foundation.

REFERENCES

1. Haddad S, Chen CA, Santangelo SL, Seddon JM. The genetics of age-related macular degeneration: a review of progress to date. Surv Ophthalmol 2006; 51:316-63.
2. Thakkinstian A, Han P, McEvoy M, Smith W, Hoh J, Magnusson K, Zhang K, Attia J. Systematic review and meta-analysis of the association between complement factor H Y402H polymorphisms and age-related macular degeneration. Hum Mol Genet 2006; 15:2784-90.
3. Okamoto H, Umeda S, Obazawa M, Minami M, Noda T, Mizota A, Honda M, Tanaka M, Koyama R, Takagi I, Sakamoto Y, Saito Y, Miyake Y, Iwata T. Complement factor H polymorphisms in Japanese population with age-related macular degeneration. Mol Vis 2006; 12:156-8.
4. Gotoh N, Yamada R, Hiratani H, Renault V, Kuroiwa S, Monet M, Toyoda S, Chida S, Mandai M, Otani A, Yoshimura N, Matsuda F. No association between complement factor H gene polymorphism and exudative age-related macular degeneration in Japanese. Hum Genet 2006; 120:139-43.
5. Tocharus J, Tsuchiya A, Kajikawa M, Ueta Y, Oka C, Kawaichi M. Developmentally regulated expression of mouse HtrA3 and its role as an inhibitor of TGF-beta signaling. Dev Growth Differ 2004; 46:257-74.
6. Dewan A, Liu M, Hartman S, Zhang SS, Liu DT, Zhao C, Tam PO, Chan WM, Lam DS, Snyder M, Barnstable C, Pang CP, Hoh J. HTRA1 promoter polymorphism in wet age-related macular degeneration. Science 2006; 314:989-92.
7. Yang Z, Camp NJ, Sun H, Tong Z, Gibbs D, Cameron DJ, Chen H, Zhao Y, Pearson E, Li X, Chien J, Dewan A, Harmon J, Bernstein PS, Shridhar V, Zabriskie NA, Hoh J, Howes K, Zhang K. A variant of the HTRA1 gene increases susceptibility to age-related macular degeneration. Science 2006; 314:992-3.
8. Armitage P. Statistical methods in medical research. New York: Wiley; 1971.
9. Scheffe, H. The Analysis of Variance. Wiley & Sons, New York, 1964.
10. Schmidt S, Hauser MA, Scott WK, Postel EA, Agarwal A, Gallins P, Wong F, Chen YS, Spencer K, Schnetz-Boutaud N, Haines JL, Pericak-Vance MA. Cigarette smoking strongly modifies the association of LOC387715 and age-related macular degeneration. Am J Hum Genet 2006; 78:852-64.
11. Rivera A, Fisher SA, Fritsche LG, Keilhauer CN, Lichtner P, Meitinger T, Weber BH. Hypothetical LOC387715 is a second major susceptibility gene for age-related macular degeneration, contributing independently of complement factor H to disease risk. Hum Mol Genet 2005; 14:3227-36.
12. Jakobsdottir J, Conley YP, Weeks DE, Mah TS, Ferrell RE, Gorin MB. Susceptibility genes for age-related maculopathy on chromosome 10q26. Am J Hum Genet 2005; 77:389-407.

The print version of this article was created on 4 Apr 2007. This reflects all typographical corrections and errata to the article through that date. Details of any changes may be found in the online version of the article.

31 Animal Models for Eye Diseases and Therapeutics

Takeshi Iwata and Stanislav Tomarev

ABSTRACT

It is believed that more than 80% of the information our brain receives comes from the visual system. Dysfunction of the visual system can significantly lower the quality of life. The most prevalent causes of visual impairment are cataracts, glaucoma, and age-related macular degeneration (AMD), which is responsible for 69% of blindness globally. In spite of the high incidence of AMD and glaucoma, a limited amount of information is available on the underlying pathological mechanisms causing these diseases. Because experimental studies of AMD and glaucoma are limited in humans, the availability of animal models is very valuable to investigate molecular mechanisms and to test new therapeutic interventions. Appropriate animal models, such as monkey, mouse, rat, and zebrafish, facilitate the identification of new genes involved in the pathology and elucidate the genetic relationships between causative and modifier genes. In this chapter the advantages and difficulties of using animal models for vision research will be discussed. Several animal models including a primate model with defined macula for AMD research and genetically modified mice models for glaucoma research will be introduced.

Key Words: Vision, Age-related macular degeneration, Retina, Macula, Drusen, Glaucoma, Retinal ganglion cells, Optic nerve.

VISUAL IMPAIRMENT AND IMPORTANCE OF ANIMAL MODELS FOR EYE DISEASES

It is believed that more than 80% of the information our brain receives comes from the visual system. Dysfunction of the visual system can alter the normal human life style and significantly lower the quality of life. The causes of visual impairments and blindness vary among ethnic groups and the global regions where they live. There are many causes of visual impairments including diabetic complications, infections, and trauma; however the most prevalent causes of visual impairment are cataracts, glaucoma, and age-related macular degeneration (AMD). According to the World Health Organization, there were more than 161 million visually impaired individuals in 2002; 124 million of this group had low vision and 37 million were blind (http://www.who.int/mediacentre/factsheets/fs282/en/index.html) (Figure 31–1).

Cataract, glaucoma, and AMD are responsible for 69% of blindness globally. Although cataracts are the leading cause of blindness worldwide, recent advances in cataract surgery have significantly reduced the visual impairments caused by cataracts, especially in developed countries. Glaucoma, an optic neuropathy, is often associated with elevated intraocular pressure and is responsible for blindness in 6.7 million people across the world. Glaucoma is more common in individuals of African ancestry, and the incidence of glaucoma increases with age.

The most prevalent eye disease for elderly Europeans and Americans is AMD. This degenerative disease progresses from retinal deposits called drusen to neovascularization and retinal hemorrhages resulting in irreversible loss of central vision.

In spite of the high incidence of AMD and glaucoma, a limited amount of information is available on the underlying pathological mechanisms causing these diseases. Obtaining tissues for any disease is often difficult, and even when obtained, they may not be informative because the tissues are usually collected many hours or even days after death. Because experimental studies of AMD and glaucoma are limited in humans, the availability of animal models is very valuable because they can be used to investigate the molecular mechanisms causing these diseases and to test new therapeutic interventions. Animal models, compared to other experimental methods, e.g., cell and organ cultures or postmortem models, allow the study of different pathological factors and therapeutic treatments under *in vivo* conditions, i.e., with the visual and other systems of the body intact. Appropriate animal models, e.g., monkey, mouse, and zebrafish, also facilitate the identification of new genes involved in the pathology as well as elucidate the genetic relationships between causative and modifier genes. Equally important, specific genes can be altered in these models. Thus, it is possible to induce mutations in animals, and then search for specific phenotypes, e.g., abnormal intraocular pressure (IOP) and retinal ganglion cell degeneration. Subsequently, the affected genes can be identified by standard genetic procedures.

Many animal models of AMD and glaucoma have been developed in different mammalian and nonmammalian species. None of these models is a perfect reproduction of the human disease, and when choosing the animal model for research, the investigator should evaluate the following: (1) the similarity of the visual system of the model to that of humans, especially the eye; (2) the similarity of the time course of pathological changes in the model and in human eyes; (3) the ability to perform genetic manipulations; (4) the training required to produce affected animals; (5) the size of the eye; (6) the availability and difficulties in the

From: *Source Book of Models for Biomedical Research*
(P. M. Conn, ed.), © 2007 Humana Press Inc., Totowa, NJ.

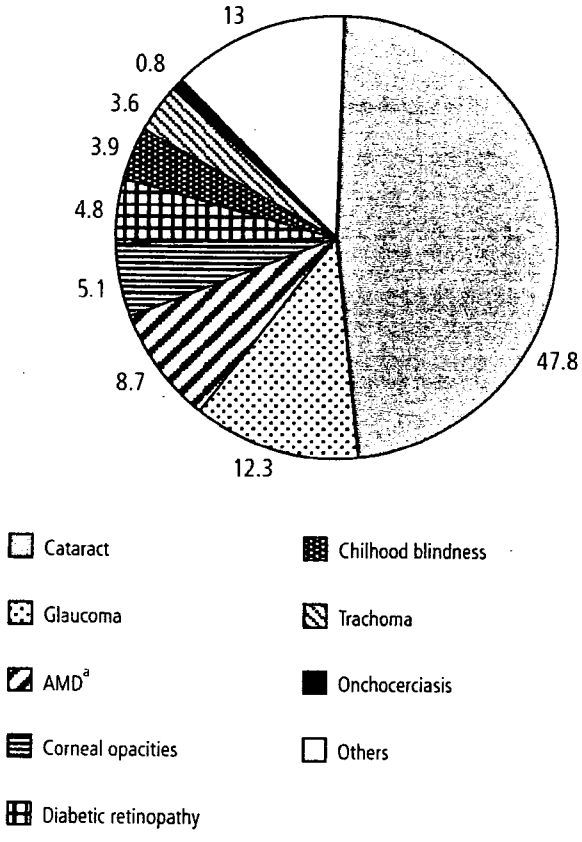

[a]AMD = Age-related macular degeneration.

WHO 04.138

Figure 31–1. Global causes of blindness as a proportion of total blindness in the year 2002 (WHO). AMD, age-related macular degeneration.

methods of analysis; (7) the availability of animals; and (8) the cost.

AGE-RELATED MACULAR DEGENERATION

INTRODUCTION The retina is composed of nine layers of neural and glial cells that are arranged concentrically at the posterior pole of the eye. Incoming light is focused on the central area of the retina called the fovea, which is located in the center of the macular area (Figure 31–2). In humans, the size of the macula is approximately 6 mm in diameter (Figure 31–3). The outer (posterior) surface of the retina is covered by a monolayer of retinal pigment epithelial (RPE) cells that forms a diffusion barrier between the neural retina and the choroidal blood supply. The RPE regulates the transport of proteins to the retina and controls the hydration and ionic composition of the subretinal space. The physiological condition of the RPE is closely associated with the pathogenesis of AMD.

AMD is a blinding disorder characterized by a marked decrease in central vision associated with RPE atrophy with or without choroidal neovascularization (CNV). Many factors, including genetic, behavioral, and environmental, are involved in this disease. AMD is characterized by the degeneration of cone photoreceptors in the foveal region of the retina resulting in a decrease of central visual acuity. The progressive impairment of the RPE cells and damage to Bruch's membrane and choriocapillaris results in retinal atrophy and photoreceptor dysfunction. In some cases, CNV develops, and the new vessels penetrate Bruch's membrane and pass into the subretinal space.

Two types of AMD are recognized: the nonneovascular type is called the dry-type AMD and includes more than 80% of the cases; the neovascular type is called the wet-type AMD and it is progressive with a higher probability of blindness. The prevalence of AMD differs considerably among the different ethnic groups, but the incidence increases with age in all groups. A lower prevalence of AMD has been reported in individuals of African ancestry than of Anglo-Saxon ancestry. Other risk factors for AMD are cigarette smoking, obesity, hypertension, and atherosclerosis.

EPIDEMIOLOGY AND GENETICS Extensive epidemiological studies have shown a genetic component for AMD. Thus, twin studies have shown a higher concordance for AMD in monozygotic twins than in dizygotic twins.[1–3] In addition, first-degree relatives of individuals with AMD have a 2- to 4-fold higher incidence of AMD than individuals without a family history of AMD. Genetic segregation studies have also shown a genetic effect that accounts for approximately 60% of AMD with a single major gene accounting for about 55% of the risk of developing

AMD. Overall, the data have suggested that the etiology of AMD has a significant genetic component. Only a small proportion of the families with AMD shows Mendelian inheritance, and the majority of the individuals inherit AMD in a complex multigene pattern.

There have been a number of attempts to identify the genes that cause AMD. With the help of the haplotype marker project (HapMap Project), genome-wide scanning has identified at least 13 loci linked to AMD on different chromosomes.[4–6]

Recently, a polymorphism of complement factor H gene (*Y402H*) was shown to be associated with an increased risk for AMD.[7–10] These results were confirmed in many of the countries with large white populations but not in Japan.[11,12] This gene is located on chromosome 1q25-31 where one of the candidate loci was identified by linkage studies. Another recent study reported that a haplotype association of tandemly located complement 2 and factor B was protective for AMD.[13]

PATHOLOGY AND BIOCHEMISTRY The early stage of the dry-type AMD is characterized by a thickening of Bruch's membrane, aggregation of pigment granules, and increasing numbers of drusen. The thickening of Bruch's membrane obstructs its function as a "barrier" between the choroid and the RPE that protects the neural retina from the choriocapillary. Drusen are small yellowish-white deposits that are composed of lipids, proteins, glycoproteins, and glycosaminoglycans. They accumulate in the extracellular space and the inner aspects of Bruch's membrane (Figure 31–3). Drusen are not directly associated with visual loss but represent a risk factor for both the dry-type and wet-type AMD. The classification of hard and soft drusen is based on their size, shape, and color; hard drusen are yellowish with diameters <50 μm and are found in eyes that are less likely to progress to advanced stages of the disease, while soft drusen are darker yellow and larger in size, and are found in eyes more likely to progress to more advanced stages of AMD. A small percentage of dry-type AMD patients progress to the late stage of the wet-type AMD that is characterized by geographic atrophy or detachment of RPE and the development of CNV in the macular region. The presence of a CNV is the factor that most damages the neural retina because the newly developed vessels grow from the choriocapillaris through Bruch's membrane and extend laterally through the RPE cell layer (classic CNV) or extend between the inner Bruch's membrane and RPE (occult CNV). In advanced stages of AMD, the CNV and fluid leaked into the subretinal or intraretinal regions lead to cell death and retinal detachment.

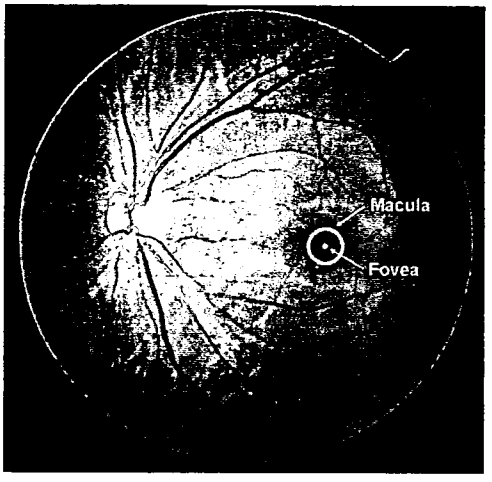

Figure 31–3. Fundus photograph of a normal human retina showing the location of the macula and the fovea.

Recent analyses of the progression of drusen have provided important clues that help understand the molecular pathology of AMD. Using both immunohistochemistry and proteomic techniques, the materials in drusen were found to be composed of molecules that mediate inflammatory and immune processes.[14,15] These molecules include components of the complement pathway and modulators of complement activation, viz. vitronectin, clusterin, membrane cofactor protein, and complement receptor-1. In addition, molecules triggering inflammation, viz. amyloid P component, α_1-antitrypsin, and apolipoprotein E, were identified in drusen. Cellular debris from macrophages, RPE cells, and choroidal dendritic cells has also been identified in drusen. On the other hand, crystallins, EEFMP1, and amyloid-β have been found at

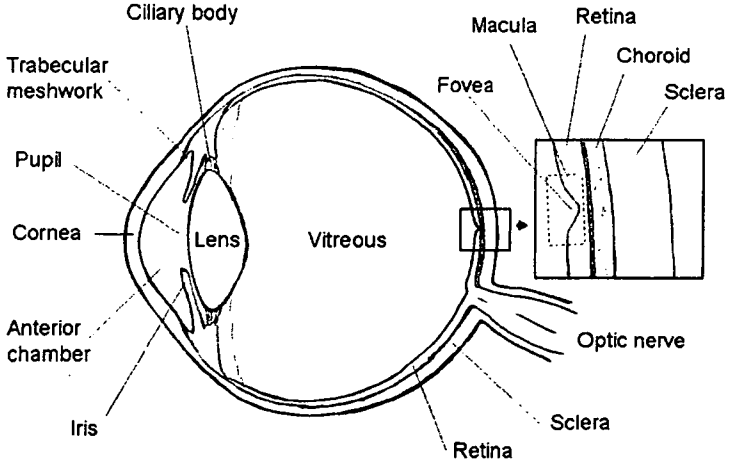

Figure 31–2. Schematic diagram of the human eye.

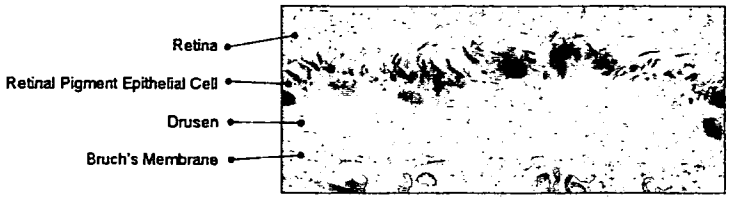

Figure 31–4. Retinal histological section showing the accumulation of drusen between the retinal pigment epithelium and Bruch's membrane in a primate model of AMD.

higher levels in drusen from individuals unaffected by AMD. The presence of immunoreactive proteins and the oxidative modifications of many proteins in drusen imply that both oxidation and immune functions are involved in the pathogenesis of AMD.

All of these findings suggest that complement activation triggers innate immune responses in the subretinal space. The codistribution of immunoglobulin G (IgG) and terminal complement complexes in drusen indicate that immune responses that directly target antigens in retinal cells might also be occurring. Antiretinal autoantibodies have been reported in a number of ocular disorders, e.g., macular degeneration in an aged monkey model.

ANIMAL MODELS Access to appropriate biological materials from affected donors at different stages of a disease is an absolute necessity for the study of mechanisms underlying the disease process. However, because it is nearly impossible to obtain retinal tissues from patients or controls, the development of animal models becomes crucial for investigating the biological pathways involved in the progression of the disease and for the development of therapeutic strategies.

Over the past few years, genetic engineering techniques have generated a number of animal models of AMD in mice, rats, rabbits, pigs, and dogs.[16] However, in mammals, a well-defined fovea is found only in primates (humans and monkeys), and a search for a monkey line affected with macular degeneration has been persistent for a long time.

A monkey with macular degeneration was first described by Stafford *et al.* in 1974. They reported that 6.6% of the elderly monkeys they examined showed pigmentary disorders and drusen-like spots.[17] El-Mofty *et al.* reported that the incidence of maculopathy was 50% in a colony of rhesus monkeys at the Caribbean Primate Research Center of the University of Puerto Rico.[18] At the Tsukuba Primate Research Center (Tsukuba City, Japan), Suzuki *et al.* found a single cynomolgus monkey (*Macaca fascicularis*) in 1986 with a large number of small drusen around the macular region (Figure 31–4).[19–21] This single affected monkey has multiplied to a large pedigree of more than 65 affected and 210 unaffected monkeys (Figure 31–5). Drusen were observed in the macular region as early as 1 year after birth, and the numbers increased and spread toward the peripheral retina throughout life. No histological abnormalities have been found in the retina, retinal vessels, or choroidal vasculatures of the eyes with drusen. Immunohistochemical and proteomic analyses of the drusen from these monkeys showed that the drusen were very similar to those in other monkeys with aged macular degeneration sporadically found in older monkeys and also with human drusen.[22,23] These observations by Umeda *et al.* have shown that the Tsukuba monkeys produce drusen that are biochemically similar to those in human AMD patients, but the development of the drusen occurs at an accelerated rate of over 25 times. Currently, 240 loci of the cynomolgus monkey are being investigated to try to identify the disease-causing gene and to understand the biological pathways leading to complement activation.

The eyes of monkey are structurally similar to human eyes, which make them extremely valuable for macular degeneration studies. However, there are limitations in using this species over other laboratory animals. Monkeys have a relatively longer life span, have a longer gestation period, have lower birth numbers resulting in a slower rate of expanding the pedigree, and are more difficult to genetically manipulate; in addition, the cost of maintenance is high. In other laboratory animals, the differences in the eye structure, lack of a fovea, and a low cone-to-rod ratio compared to humans have been considered to be a disadvantage for using them as AMD models. However, they are easier to manipulate genetically and easier and less expensive to maintain. This has made the development of a mouse model of AMD very attractive, and a number of mouse AMD models have been reported recently.

The mouse model described by Ambati *et al.* is deficient either in monocyte chemoattractant protein-1 or its cognate C–C chemokine receptor-2. These mice were found to develop the cardinal

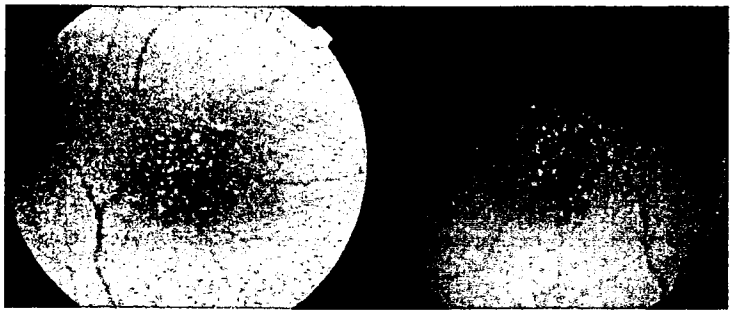

Figure 31–5. Photographs of the fundus of two monkeys with AMD in the Tsukuba Primate Research Center showing drusen.

features of AMD including accumulation of lipofuscin in drusen beneath the RPE, photoreceptor atrophy, and CNV.[24] An impairment of macrophage recruitment allowed the accumulation of C5a and IgG, which leads to the production of vascular endothelial growth factor by the RPE cells and the development of CNVs.

Another mouse model that has three known AMD risk factors—age, high-fat cholesterol-rich diet, and expression of human apolipoprotein E (apoE2, apoE3, andapoE4)—has been developed.[25] ApoE4-deficient mice are severely affected showing diffuse subretinal pigment epithelial deposits, drusen, thickened Bruch's membrane, and atrophy, hypopigmentation, and hyperpigmentation of the RPE.

Oxidative stress has long been linked to the pathogenesis of AMD. Imamura, *et al.* reported Cu, Zn-superoxide dismutase (SOD1)-deficient mice that had features typical of AMD in humans. Senescent $Sod1^{-/-}$ mice had drusen, thickened Bruch's membrane, and choroidal neovascularization.[26] The number of drusen increased with age and also after exposure of young $Sod1^{-/-}$ mice to excess light. The retinal pigment epithelial cells of $Sod1^{-/-}$ mice showed oxidative damage, and their β-catenin-mediated cellular integrity was disrupted. These findings suggested that oxidative stress may affect the junctional proteins necessary for the barrier integrity of the RPE. These observations strongly suggested that oxidative stress may play a major role in AMD.

The complement components, C3a and C5a, are present in drusen, and were observed in Bruch's membrane of a laser-induced CNV mice model. Neutralization of C3a or C5a by antibody or by blockade of their receptors by a complement inhibitor significantly reduced the CNV. These observations revealed a role of immunological mechanisms for angiogenesis and provided evidence for future therapeutic strategies for AMD.

Although the pathology of AMD is pronounced in the macula area, it is not confined to this region. Characteristics of human AMD such as thickening of Bruch's membrane, accumulation of drusen, and CNV have been observed in mouse models. Nevertheless, the primate model will still be the choice for AMD studies, especially at the stage when new therapeutic methods are tested and evaluated for the first time. However, it would be wise and more productive to study both primate and mouse models in AMD research. This will be necessary to determine the mechanisms underlying the disease and to identify clinical and molecular markers for the early stages of AMD. The findings from these studies will provide critical information needed to develop therapies for AMD.

GLAUCOMA

OVERVIEW Glaucoma is a heterogeneous group of complex neurodegenerative disorders that is characterized by the constriction of the visual field, death of retinal ganglion cells (RGCs), and a pathognomonic deformation of the optic nerve head (ONH) known as glaucomatous cupping. Glaucomas are classified into three main types: open-angle, closed-angle, and congenital glaucoma. Each of these types is subdivided into primary and secondary types.

EPIDEMIOLOGY AND GENETICS Primary open-angle glaucoma (POAG) is the most common form of glaucoma; it occurs in about 4.5 million people worldwide and accounts for 12% of all global blindness. By the year 2020, over 11 million people will be blind from primary glaucoma.[28] POAG is often, but not always, associated with elevated IOP, which is one of the main risk factors in glaucoma. However, about a third of all patients with POAG develop the disease without an IOP elevation, and in these patients, the IOP is continuously below 21 mm Hg. This form of POAG is called normal tension or low tension glaucoma (NTG). A reduction of the IOP, even in cases of NTG, is the main, clinically proven, treatment for glaucoma.

ANIMAL MODELS Among the different animal models of glaucoma, the monkey models are superior because of the anatomical similarity of the monkey eyes to human eyes and the phylogenetic similarities of these two species. At the same time, monkeys are extremely expensive and experiments on them require a highly skilled team of investigators.

Most of the existing animal models of POAG, including the monkey models, are based on the elevation of the IOP. An elevation of the IOP develops from an imbalance between aqueous humor production and outflow. Aqueous humor, a fluid produced by the ciliary body of the eye, drains out of the eye and into the blood circulatory system. The eye's outflow system consists of a series of endothelial cell-lined structures that include the trabecular meshwork (TM), Schlemm's canal (SC), which serves as a collector vessel, and the episcleral venous system (Figure 31–6). In most glaucoma models, the IOP is elevated as a result of a reduction or blockage of the aqueous humor outflow. In monkeys, an elevation of IOP is commonly induced by laser photocoagulation of the TM.[29,30] Several days after the laser treatment, the IOP increases and this elevation may last for more than a year, although more than one laser session is usually required to achieve a sustained elevation of the IOP. The IOP in treated eyes is usually between 25 and 60 mm Hg.

Other methods to elevate the IOP in monkey eyes include the anterior chamber injection of ghost red cells,[31] latex microspheres,[32] cross-linked polyacrylamide gels,[33] and enzymes.[34] Topical steroids have also been shown to elevate the IOP.[35] These latter treatments produce less consistent elevations than laser photocoagulation.[36]

Monkey glaucoma models have been shown to have changes in the optic disk, optic nerve, RGC, and nerve fiber layers similar to those observed in glaucomatous human eyes. Apoptosis was shown to be the cause of the RGCs death in a monkey photocoagulation model,[37] and apoptosis was later confirmed to be the cause in other animal models and in humans with glaucoma. Monkey glaucoma models have also been successfully used to study changes in the retinal gene expression pattern 30 days after laser photocoagulation of the TM,[38] and to test the effectiveness of new classes of hypotensive drugs.[36]

Rodent became the animal of choice when large numbers of animals were required, e.g., when examining the mechanism of RGC degeneration and neuroprotection. Several rat models of elevated pressure-induced optic nerve damage have been developed during the past decade, and they have been used to study changes in the retina and the optic nerve. Rats are easy to handle and the relatively large size of their eyes allows multiple, awake measurements of the IOP with commercially available equipment.[39] This latter is important because it is well documented that general anesthesia induces a rapid decrease in the IOP. Although there are certain differences in the structure of the rat and human eyes, all of the eye structures affected in glaucomatous human eyes exist in the rat eye.

In rat models, the IOP elevation is achieved by injection of concentrated saline solution into the episcleral veins.[40] laser

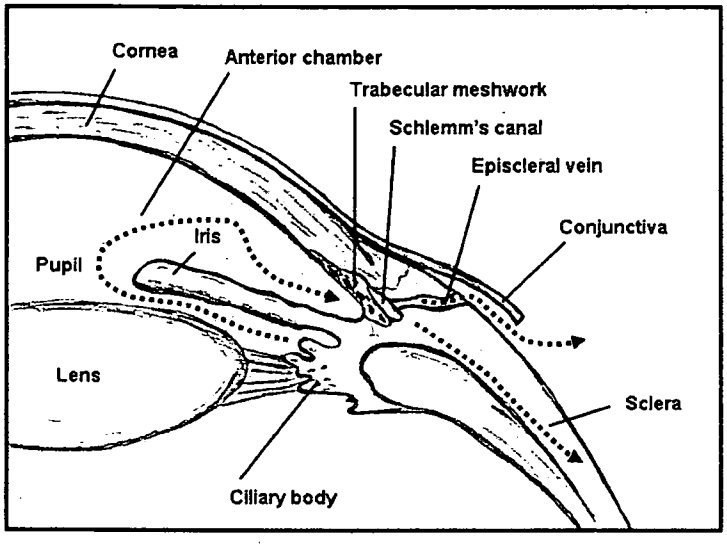

Figure 31–6. Schematic diagram of the anterior segment of the eye showing the trabecular meshwork and uveoscleral outflow pathways of aqueous humor.

photocoagulation of the TM after an injection of Indian ink into the anterior chamber,[41] laser photocoagulation of the TM,[42] and laser cauterization of episcleral veins.[43] All of these methods that lead to an elevation of the IOP require special training of the investigators.

Successful treatment of the eye leads to a rapid elevation of the IOP, although the level of elevation varies from eye to eye. Saline injection generally produces a wide range of IOP elevation from a very minimal rise to a 2-fold increase over the IOP in control eyes. The elevation of the IOP generally lasts for several weeks, and a second laser treatment is often required in the photocoagulation method to maintain an elevated IOP for more than 3 weeks.

A chronic elevation of the IOP in rats leads to apoptosis of the RGCs, degeneration of the optic nerve fibers, and remodeling of the ONH similar to those observed in human glaucomatous eyes.[40,44–45] Rat models of glaucoma have been used to study the effects of elevated IOP on the electroretinogram,[46] neuroprotective drugs,[47] and molecular changes in the retina and optic nerve using the candidate gene approach and array hybridization.[48]

A mutant rat strain was reported to have unilateral or bilateral enlargement of the eyes with an IOP ranging from 25 to 45 mm Hg. In this strain of rat, cupping of the optic nerve head was detected by funduscopic examination, and the cupping was more pronounced in older animals. The number of RGCs also declined with age.[49] Unfortunately, this strain was obtained from the Royal College of Surgeons colony that has a mutation in the receptor tyrosine kinase gene, leading to degeneration of the photoreceptors. Therefore, this strain can hardly be considered a good glaucoma model.

The construction of mouse models of glaucoma has lagged behind rat glaucoma models for a long time despite the advantages of mice over rats and other mammalian species for cost-effective genetic manipulations, availability of a wide spectrum of methods, and the existence of many genetically modified strains. However, it should be remembered that mouse and human eyes have certain important differences including the arterial blood supply to the optic nerve head and the absence of a lamina cribrosa.[50] The lamina cribrosa, a collagenous scaffold supporting the optic nerve, plays a critical role in the damage/protection of the human optic nerve.

One of the main difficulties working with mice is that their eyes are much smaller than the eyes of humans and rats, and new methods had to be developed to measure the IOPs in mice. To date, several invasive and noninvasive methods of IOP measurements have been developed for mice. The first remains one of the most reliable and accurate methods and does not depend upon the mechanical properties of the cornea. It involves the insertion of a glass microneedle connected to a pressure transducer into the anterior chamber of the eye. Using this method, it was shown that common mouse strains have different IOP between 10 and 20 mm Hg.[51] Other methods of IOP measurements in mice were later developed including noninvasive techniques. Noninvasive methods allow multiple IOP measurements to be completed in a short period of time, but the results of these measurements may depend upon mechanical properties of the cornea. To obtain reliable IOP readings, all of the described techniques require training.

Transgenic and gene-targeted knockout approaches have been used to develop several mouse models of glaucoma. The main advantage of these models is that the animals with the mutated gene provide a more uniform elevation of the IOP and damage to the retina and optic nerve similar to that found with surgically induced elevated IOPs. A large number of animals can be produced, and once a mutant mouse line is obtained, no special training is needed to produce more affected mice.

Several lines of transgenic mice have been developed that contained BAC DNAs with a mouse Tyr423His point mutation and Tyr437His point mutation of the human myocilin (Myoc) genes. The Tyr437His mutation in the Myoc gene leads to severe glaucoma in humans, and the mouse Tyr423His mutation corresponds to this human mutation. Expression of mutated mouse Myoc in the ocular drainage structures led to moderate (about 2 mm Hg during the day and 4 mm Hg at night) elevation of the

IOP and progressive degenerative changes in the peripheral RGC layer and optic nerve that resembled glaucomatous changes in human eyes.[52] In 1-year-old animals, the peripheral retina of transgenic mice had approximately 20% fewer RGCs than the peripheral retina of control littermates.

Transgenic mice with a targeted mutation in the gene for the α_1-subunit of collagen type I have also been constructed. This mutation blocks the cleavage of collagen by matrix metalloproteinase-1. Transgenic mice expressing mutated collagen had elevated IOPs. The difference in the IOP between control and transgenic mice gradually increased to a maximum of 4.8 mm Hg at 36 weeks. Because these mice had progressive optic nerve axon loss with normal organization of the drainage structures, it has been suggested that they may be used as a mouse model of POAG.[53]

Recent data have demonstrated that transgenic mice expressing mutated optineurin under the control of the ubiquitous ROSA26 promoter develop optic nerve cupping and death of the RGCs without elevation of the IOP.[54] These transgenic mice may represent the first animal model of NTG.

The surgical methods used to produce rat glaucoma models have also been used in mice. However, performing surgery on the mouse eye is even more challenging than on rat eyes because of the difference in size. A significant elevation of the IOP was found in the eyes of C57BL/6J mice that had an injection of indocyanine green dye into the anterior chamber and diode laser treatment of the TM and episcleral vein region.[55] At 10 days after the surgery, the mean IOP in the operated eyes was 33.6 ± 1.5 mm Hg versus 15.2 ± 0.6 mm Hg in the control eyes. However, the IOP returned to normal 60 days after the surgery. Histological examination of the treated eyes 65 day after the surgery revealed anterior synechia, a decrease in the number of RGCs, thinning of all retinal layers, and damage to the optic nerve structures without evidence of prominent cupping.[55] A reduction in the function of the outer retinal layers, confirmed by electroretinographic studies, may indicate that this model produces more extensive changes in the retina compared to the glaucoma in humans.

Similar to the above model, an elevation of IOP was induced by argon laser photocoagulation of the episcleral and limbal veins in C57BL/6J mouse eyes[56] or by cauterization of three episcleral veins in CD1 mouse eyes.[57] During the first 4 weeks following laser treatment, the mean IOP in the treated eyes was about 1.5 times higher than in control eyes. The number of RGCs had decreased by $22.4 \pm 7.5\%$ of that in the controls at 4 weeks after treatment. Most of the TUNEL-positive apoptotic cells were detected in the peripheral retina.[56]

Cauterization of the episcleral veins led to a maximum IOP elevation within 2–9 days, and the IOP decreased progressively thereafter to reach more or less normal values after 24–33 days. There was a 20% decrease in the number of RGCs 2 weeks after the surgery.[57]

The DBA/2J strain has high IOP and has become a popular mouse model to study secondary angle-closure glaucoma. This mouse strain has mutations in two genes, *Tyrp1* and *Gpnmb*.[58] DBA/2J mice develop pigment dispersion, iris transillumination, iris atrophy, and anterior synechia. At the age of 9 months, the IOP was elevated in most mice and the elevation was accompanied by the death of the RGCs, optic nerve atrophy, and optic nerve cupping. Although no group of the RGCs was especially vulnerable or resistant to degeneration, fan-shaped sectors of dead or surviving RGC radiated from the ONH.[59] It has been suggested that axon damage at the ONH might be a primary lesion in this model.[59]

Several important observations were made from the studies on the DBA/2J model. It was shown that the proapoptotic protein BAX is required for the survival of RGCs but not for RGC axon degeneration, suggesting that BAX may be a candidate human glaucoma susceptibility gene.[60] Unexpectedly, a high dose of γ-irradiation accompanied by syngeneic bone marrow transfer protected the RGCs in DBA/2J mice.[61] Similar to the results obtained with rat and monkey models, genes involved in the glial activation and immune response were activated in DBA/2J retina as shown by array hybridization.[62]

Complement component, 1Q, was upregulated in the retina of several animal models of glaucoma as it is in human glaucoma with the timing suggesting that complement activation plays a significant role in the pathogenesis of glaucoma.[63]

Taken together, these findings confirm that animal models might be used to look for a molecular mechanism involved in glaucoma in humans.

The modulation of the activity of genes involved in the development of the anterior segment of the eye may lead to relatively rare developmental glaucomas that account for less than 1% of all glaucoma cases. Several genes have been implicated in congenital glaucoma and anterior segment disgenesis. They include *Cyp1b1*, *Foxc1*, *Foxc2*, *Pitx2*, *Lmx1b*, and *Pax6*. Several lines of mice with defects in these genes have been studied with glaucoma in mind (see Gould *et al.*[64] for a review). For example, mutation in the *CYP1B1* gene (cytochrome P450, family 1, subfamily b, polypeptide 1) may lead to primary congenital glaucoma (PCG) in humans. Although Cyp1b1 knockout mice did not develop elevated IOP, they had ocular abnormalities similar to the defects in humans with PCG, viz. small or absent Schlemm's canal, defects in the TM, and attachment of the iris to the TM and anterior synechia.

Mutations in the *FOXC1* gene, which encodes a transcription factor with a forkhead-winged-helix DNA binding domain, cause a range of eye abnormalities associated with glaucoma, e.g., iris hypoplasia, Axenfeld and Rieger anomaly, and Rieger syndrome. $Foxc1^{-/-}$ mice die at birth, while $Foxc1^{+/-}$ animals are viable but have defects in the eye drainage structures without changes in IOP. Similar eye defects were observed in $Foxc2^{+/-}$ mice. It has been suggested that $Foxc1^{+/-}$ and $Foxc2^{+/-}$ mice are useful models for studying anterior segment development and anomalies, and may allow the identification of genes that interact with *Foxc1* and *Foxc2* (or *FKHL7* and *FKHL14*) to produce a phenotype with elevated IOP and glaucoma.

Other animals, including rabbit, pig, and bovine, have also been used to develop animal models of glaucoma, but none of them is widely used for different reasons. Zebrafish became a powerful model for advanced genetic studies in vertebrates, especially in the case of complex diseases, and was proposed as a model for identification of modifier genes for glaucoma.[65]

CONCLUSIONS

In summary, animal models of glaucoma, including the most widely used rodent and monkey models, have already provided interesting new information about mechanisms of glaucoma in humans. However, it should be remembered that even in monkey models the time course of changes in the glaucomatous eyes may

K1

be significantly accelerated compared to that in human glaucomatous eyes. and all discussed models are indeed just models of glaucoma in humans. Results obtained with these models should not be automatically applied to human glaucoma and should be confirmed by testing in humans whenever possible. It has become clear that reaction to the same insult, e.g., elevated IOP, may be somewhat different in different animal models. Glaucoma studies in animals may help us identify the molecular mechanisms involved in the development of glaucoma in each particular model. By comparing these mechanisms, it may be possible to find some common mechanism that might be involved in glaucoma formation in humans. This will be extremely valuable for the development of new therapeutic approaches for the treatment and prevention of glaucoma in humans.

REFERENCES

1. Heiba IM, Elston RC, Klein BE. Klein R. Sibling correlations and segregation analysis of age-related maculopathy: The Beaver Dam Eye Study. *Genet Epidemiol* 1994:11:51–67.
2. Seddon JM. Ajani UA, Mitchell BD. Familial aggregation of age-related maculopathy. *Am J Ophthalmol* 1997;123:199–206.
3. Hammond CJ, Webster AR, Snieder H, Bird AC, Gilbert CE, Spector TD. Genetic influence on early age-related maculopathy: A twin study. *Ophthalmology* 2002:109:730–736.
4. Iyengar SK, Song D. Klein BE, Klein R, Schick JH, Humphrey J. Millard C, Liptak R. Russo K. Jun G, Lee KE, Fijal B, Elston RC. Dissection of genomewide-scan data in extended families reveals a major locus and oligogenic susceptibility for age-related macular degeneration. *Am J Hum Genet* 2004;74:20–39.
5. Schick JH, Iyengar SK, Klein BE, Klein R, Reading K, Liptak R, Millard C. Lee KE, Tomany SC, Moore EL, Fijal BA, Elston RC. A whole-genome screen of a quantitative trait of age-related maculopathy in sibships from the Beaver Dam Eye Study. *Am J Hum Genet* 2003:72:1412–1424.
6. Majewski J. Schultz DW. Weleber RG. Schain MB. Edwards AO. Matise TC. Acott TS, Ott J, Klein ML. Age-related macular degeneration—a genome scan in extended families. *Am J Hum Genet* 2003;73:540–550.
7. Klein RJ. Zeiss C, Chew EY. Tsai JY. Sackler RS. Haynes C, Henning AK, SanGiovanni JP, Mane SM. Mayne ST, Bracken MB, Ferris FL. Ott J, Barnstable C, Hoh J. Complement factor H polymorphism in age-related macular degeneration. *Science* 2005;308:385–389.
8. Edwards AO, Ritter R 3rd, Abel KJ. Manning A, Panhuysen C. Farrer LA. Complement factor H polymorphism and age-related macular degeneration. *Science* 2005;308:421–424.
9. Haines JL. Hauser MA, Schmidt S. Scott WK. Olson LM. Gallins P. Spencer KL, Kwan SY, Noureddine M, Gilbert JR. Schnetz-Boutaud N, Agarwal A, Postel EA. Pericak-Vance MA. Complement factor H variant increases the risk of age-related macular degeneration. *Science* 2005;308:419–421.
10. Hageman GS, Anderson DH, Johnson LV, Hancox LS, Taiber AJ. Hardisty LI, Hageman JL, Stockman HA. Borchardt JD, Gehrs KM. Smith RJ, Silvestri G. Russell SR, Klaver CC. Barbazetto I. Chang S. Yannuzzi LA. Barile GR. Merriam JC. Smith RT, Olsh AK. Bergeron J, Zernant J, Merriam JE. Gold B. Dean M. Allikmets R. A common haplotype in the complement regulatory gene factor H (HF1/CFH) predisposes individuals to age-related macular degeneration. *Proc Natl Acad Sci USA* 2005;102:7227–7232.
11. Okamoto H. Umeda S. Obazawa M. Minami M, Noda T. Mizota A. Honda M. Tanaka M. Koyama R. Takagi I. Sakamoto Y. Saito Y. Miyake Y. Iwata T. Complement factor H polymorphisms in Japanese population with age-related macular degeneration. *Mol Vis* 2006;12:156–158.
12. Gotoh N. Yamada R. Hiratani H, Renault V, Kuroiwa S. Monet M, Toyoda S, Chida S. Mandai M, Otani A, Yoshimura N, Matsuda F. No association between complement factor H gene polymorphism and exudative age-related macular degeneration in Japanese. *Hum Genet* 2006:120:139–143.
13. Gold B, Merriam JE, Zernant J. Hancox LS, Taiber AJ. Gehrs K. Cramer K, Neel J, Bergeron J. Barile GR. Smith RT; AMD Genetics Clinical Study Group; Hageman GS, Dean M, Allikmets R. Variation in factor B (BF) and complement component 2 (C2) genes is associated with age-related macular degeneration. *Nat Genet* 2006;38:458–462.
14. Russell SR. Mullins RF, Schneider BL, Hageman GS. Location. substructure, and composition of basal laminar drusen compared with drusen associated with aging and age-related macular degeneration. *Am J Ophthalmol* 2000;129:205–214.
15. Mullins RF, Russell SR, Anderson DH, Hageman GS. Drusen associated with aging and age-related macular degeneration contain proteins common to extracellular deposits associated with atherosclerosis, elastosis. amyloidosis, and dense deposit disease. *FASEB J* 2000;14:835–846.
16. Chader GJ. Animal models in research on retinal degenerations: Past progress and future hope. *Vision Res* 2002;42:393–399.
17. Stafford TJ. Anness SH. Fine BS. Spontaneous degenerative maculopathy in the monkey. *Ophthalmology* 1984;91:513–521.
18. El-Mofty A, Gouras P. Eisner G. Balazs EA. Macular degeneration in rhesus monkey (Macaca mulatta). *Exp Eye Res* 1978:27:499–502.
19. Nicolas MG. Fujiki K, Murayama K, Suzuki MT. Mineki R. Hayakawa M, Yoshikawa Y, Cho F. Kanai A. Studies on the mechanism of early onset macular degeneration in cynomolgus (Macaca fascicularis) monkeys. I. Abnormal concentrations of two proteins in the retina. *Exp Eye Res* 1996;62:211–219.
20. Nicolas MG. Fujiki K, Murayama K, Suzuki MT, Shindo N. Hotta Y, Iwata F. Fujimura T, Yoshikawa Y, Cho F. Kanai A. Studies on the mechanism of early onset macular degeneration in cynomolgus monkeys. II. Suppression of metallothionein synthesis in the retina in oxidative stress. *Exp Eye Res* 1996;62:399–408.
21. Suzuki MT. Terao K. Yoshikawa Y. Familial early onset macular degeneration in cynomolgus monkeys (*Macaca fascicularis*). *Primates* 2003;44:291–294.
22. Umeda S. Ayyagari R. Allikmets R, Suzuki MT, Karoukis AJ. Ambasudhan R. Zernant J, Okamoto H, Ono F, Terao K. Mizota A. Yoshikawa Y, Tanaka Y, Iwata T. Early-onset macular degeneration with drusen in a cynomolgus monkey (*Macaca fascicularis*) pedigree: Exclusion of 13 candidate genes and loci. *Invest Ophthalmol Vis Sci* 2005;46:683–691.
23. Umeda S, Suzuki MT. Okamoto H. Ono F, Mizota A, Terao K. Yoshikawa Y, Tanaka Y, Iwata T. Molecular composition of drusen and possible involvement of anti-retinal autoimmunity in two different forms of macular degeneration in cynomolgus monkey (Macaca fascicularis). *FASEB J* 2005:19:1683–1685.
24. Ambati J, Anand A. Fernandez S. Sakurai E. Lynn BC, Kuziel WA. Rollins BJ, Ambati BK. An animal model of age-related macular degeneration in senescent Ccl-2- or Ccr-2-deficient mice. *Nat Med* 2003:9:1390–1397.
25. Malek G. Johnson LV. Mace BE. Saloupis P. Schmechel DE. Rickman DW, Toth CA, Sullivan PM, Bowes Rickman C. Apolipoprotein E allele-dependent pathogenesis: A model for age-related retinal degeneration. *Proc Natl Acad Sci USA* 2005:102:11900–11905.
26. Imamura Y. Noda S. Hashizume K. Shinoda K. Yamaguchi M. Uchiyama S, Shimizu T. Mizushima Y, Shirasawa T, Tsubota K. Drusen, choroidal neovascularization. and retinal pigment epithelium dysfunction in SOD1-deficient mice: A model of age-related macular degeneration. *Proc Natl Acad Sci USA* 2006;103:11282–11287.
27. Nozaki M, Raisler BJ, Sakurai E, Sarma JV. Barnum SR. Lambris JD, Chen Y. Zhang K, Ambati BK, Baffi JZ, Ambati J. Drusen complement components C3a and C5a promote choroidal neovascularization. *Proc Natl Acad Sci USA* 2006;103:2328–2333.
28. Quigley HA. Broman AT. The number of people with glaucoma worldwide in 2010 and 2020. *Br J Ophthalmol* 2006:90:262–267.
29. Gaasterland D. Kupfer C. Experimental glaucoma in the rhesus monkey. *Invest Ophthalmol Vis Sci* 1974;13:455–457.

K1